Circuits, Systems, and Signal Processing
https://doi.org/10.1007/s00034-026-03606-2

Passivity Disturbance Analysis for Delayed Discrete-Time System with Stochastic Terms via Quantized Event-Triggered and Deception Attack

Gokulam Mariappan[1] · Muthukumar Shanmugam[1] · Vadivel Rajarathinam[2] · Nallappan Gunasekaran[3]

Received: 28 December 2025 / Revised: 2 April 2026 / Accepted: 3 April 2026

Abstract

This work addresses the passivity disturbance analysis for delayed discrete-time systems under quantized event-triggered communication and deception attacks. To ease network load and minimize communication overhead, an event-triggered mechanism and a logarithmic quantizer are introduced individually. The influences of event-triggered, quantization, stochastic terms, and cyber attacks are combined within a single unified framework and by designing a suitable Lyapunov–Krasovskii functional (LKF), we establish sufficient conditions that ensure asymptotic stability of the system. The proposed method derives stability and passivity conditions that allow larger admissible delays and stronger tolerance to disturbances, leading to improved control performance. Building on these results, a resilient event-triggered control approach is formulated using linear matrix inequalities (LMIs). In addition, when external disturbances occur, further conditions are derived to guarantee system passivity. In the end, the proposed method demonstrates its effectiveness through four numerical simulation examples, which include comparative studies that assess control accuracy, achieving

✉ Muthukumar Shanmugam
sivagirimuthu@gmail.com

✉ Vadivel Rajarathinam
vadivelsr@yahoo.com

Gokulam Mariappan
gokulam.mmm@gmail.com

Nallappan Gunasekaran
gunasmaths@gmail.com

[1] Department of Mathematics, Sri Ramakrishna Mission Vidyalaya College of Arts and Science, Coimbatore 641020, Tamil Nadu, India

[2] Department of Mathematics, Faculty of Science and Technology, Phuket Rajabhat University, Phuket 83000, Thailand

[3] Eastern Michigan Joint College of Engineering, Beibu Gulf University, Qinzhou 535011, Guangxi, China

Published online: 24 April 2026

an approximately 83% reduction in communication needs as compared to traditional control schemes, and maintaining computational efficiency.

Keywords Discrete time · Event-Triggered · Lyapunov-Krasovskii functional · Time-Varying Delay · Passivity Analysis

1 Introduction

In recent years, discrete-time systems (DTSs) commonly appear in modern control applications where measurements and control signals are handled in digital form. Such systems provide an appropriate modeling framework for implementations based on computers, embedded platforms, and networked control architectures. Discrete-time systems offer advantages such as flexibility, high efficiency, and high accuracy, and in engineering practice, discrete models incorporating external disturbances are more commonly employed [33],[18]. Discrete time models are provided system descriptions compatible with the behavior under sampling and holding, as well as allow for advanced control design to be seen at intermediate levels between theory and implementation, given in [1]. New Lyapunov functionals and delay-dependent techniques are used to establish less conservative stability conditions for DTSs with time-varying state delays, which significantly improve upon earlier results in [5]. The work [7] focused on a free-weighting matrix approach to output feedback control for linear DTSs with interval time-varying delays is developed, leading to the development of new stability criteria and controller syntheses. In [29], [30], the authors investigate a robust H_∞ control method for discrete-time T–S fuzzy switched memristive stochastic neural networks and an event-triggered switched system with transmission delays. We observe that robust synchronization DTS analyzed in [25],[31] under actuator and nonlinear perturbations.

The study of passivity in discrete-time systems with delays has gained significant interest among researchers in recent years. A focus on passivity offers a natural energy-based perspective for the analysis and design of control systems, since passive networks yield or dissipate but do not generate energy, and it has several attractive features in the context of control theory applications are proposed in [19]. In article [20], the authors propose a sufficient condition of passivity and saturation overflow of delayed DTS under exogenous disturbance. A general free-matrix-based summation inequality is proposed in [21]. With the help of the passivity and passification case discussed in [27], the authors are presented in article [23], the event-triggered synchronization problem for delayed neural networks and provide an analysis for the stable interaction of clustered multi-agent systems. In [8],[24], A passivity-based stabilizing controller for robots to ensure robust operation under dynamic uncertainties are explained. The articles [9],[2], a passivity-based method to accelerate convex optimization, linking control-theoretic energy concepts with algorithmic convergence, were proposed. In this paper, the block diagram of the control problem based on [30] for networked systems under deception attacks as it is addressed is depicted in Figure 1.

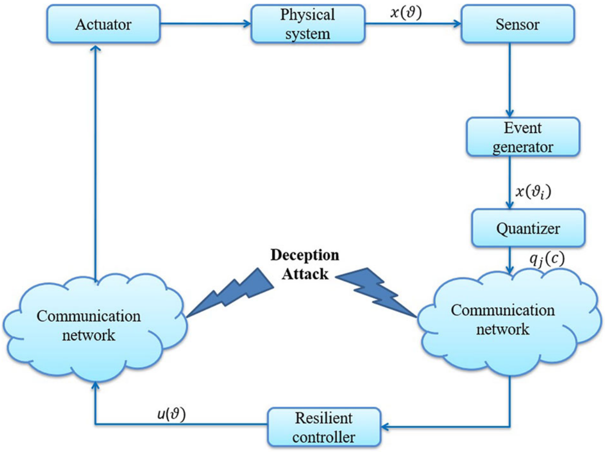

Fig. 1 The DTS with quantizer under deception attack [30]

The communication scheme is only in connection with the time-triggered structure, where a calibrated sampling period is applied. With the increasingly wide use of cyber–physical systems and networked control systems (NCS), event-triggered control (ETC) has been considered in [22] (see Tables 1 and 2), as a useful paradigm to alleviate communication burden and enhance resource utilization, it has the advantages of saving computing resources and reducing communication occupancy. In the work [14],[34] quantized event-triggered synchronization of discrete chaotic neural networks in the presence of stochastic deception attacks, and some sufficient conditions are considered. In [32], strict dissipativity-based synchronization is established for delayed static neutral neural networks with an event-triggered scheme, by which stability, communication cost, and networked multi-agent applications have been proved. The papers [26],[6] are investigated to outline current progress and future research directions under the periodic disturbances and the nonlinear adaptive ETC. In paper [15], the author's are explained markovian switching rules, ETC approach, and cyber attacks for synchronization under external perturbations. Resilient control of nonlinear discrete-time state-delay systems subject to uncertainties and external disturbances is utilized in [28],[17]. On fault estimation and control of unknown discrete-time systems using a data-driven parameterization approach is presented in [13]. In article [4], a theorem-based approach using the matrix exponential and spectral radius to efficiently and reliably assess Hurwitz stability. In paper [3], the authors are focused on bounded input and bounded output stability analysis for linear type invariant systems under the basis of Howland's eigenvalue separation theorem. The authors investigated a hybrid neuro-fuzzy transfer function, an independent neutral fuzzy nonlinear model, and a Wiener output-error nonlinear system to identify the time-delay model of a Hammerstein–Wiener system, where the static and dynamic components are represented using the former approaches in [12],[11],[10]. To the best of the author's knowledge, passivity disturbance analysis for delayed discrete-time under ETC and deception attack has not been studied so far, which motivates the present study.

Table 1 Comparison of Quantized ETC with passivity of DTS

References	Passivity	Quantized	Event-Triggered	Resilient
[21]	✓	✗	✗	✗
[27]	✗	✗	✓	✗
[26]	✓	✗	✓	✓
[6]	✗	✗	✓	✗
[17]	✗	✗	✗	✓
Our work	✓	✓	✓	✓

Inspired by the above literature, this study introduces quantized event-triggered control for DTS with time delay affected by stochastic deception attacks and passivity disturbance is considered. A sufficient condition is derived to ensure the asymptotic stability and passivity performance of the addressed system by LKF. The main contributions of this work are as follows:

1. The quantized ETC design technique has been developed for DTSs via passivity disturbance and stochastic deception attack.
2. We examined a problem for DTSs, where the control inputs are simultaneously characterized by quantization and cyber attack.
3. Asymptotic stability is analyzed using the LKF. Moreover, important lemmas and definitions are used to solve and obtain control gains through LMI for DTSs.
4. The effectiveness and applicability of the developed conditions are demonstrated through various examples. The proposed method is less conservative, and comparison results are illustrated in the numerical examples section.

The paper is organized as follows. System characterization, definitions, and lemmas are presented in Section 2. Sufficient conditions for asymptotic stability and passivity constraints with ETC of the system under consideration are given in Section 3. Three illustrative examples and an application are provided in Section 4. The conclusion is proposed in Section 5.

Notation: In a matrix $*$ denotes symmetric term. $\mathbb{X}^T$ and $\mathbb{X}^{-1}$ represent transpose and inverse of matrix $\mathbb{X}$. Positive definite matrix (semi positive definite) $\mathbb{X}$ expressed as $\mathbb{X} > 0$ ($\mathbb{X} \geq 0$). $\boldsymbol{I}$ represents identity matrix of the appropriate dimensions, $sym\,[\mathbb{X}] = \mathbb{X} + \mathbb{X}^T$. $\mathbb{R}^m$ and $\mathbb{R}^n$ represent m-dimensional and n-dimensional Euclidean space, respectively. $\mathbb{R}^{n\times m}$ is the set of real $n \times m$ matrices. $diag\,\{...\}$ represents block diagonal matrix. $||.||$ stands for the Euclidean norm.

2 System Description

The DTS along quantized ETC as follows

$$\boldsymbol{x}(\vartheta + 1) = \boldsymbol{A}\boldsymbol{x}(\boldsymbol{\vartheta}) + \boldsymbol{A_d}\boldsymbol{x}(\boldsymbol{\vartheta} - \boldsymbol{d}(\boldsymbol{\vartheta})) + \boldsymbol{B}u(\vartheta), \tag{1}$$

Table 2 Overview of related research studies

References	Main contribution	Relevance to current work
[25]	Studied event-triggered H_∞ of delayed discrete-time recurrent neural network.	Our work applies ETC to DTS to reduce network communication and burden.
[8]	Investigated passivity-based control for dynamical systems by switching property.	Our focuses control with passivity disturbance for DTS with cyber attacks.
[22]	Presented resilient sampled data control strategy with external disturbance.	Our work proposed a resilient ETC with external disturbance under cyber attacks.
[14]	Explored event-triggered synchronization of chaotic neural networks with deception attack.	Our articles employ an event-triggered controller for delayed DTS under deception attack.
[6]	Developed distributed coordination of ETC for micro grids and automated vehicles applications.	Our paper analyzes ETC for delayed DTS under stochastic deception attack with its application.

when an external disturbance $\bar{\boldsymbol{w}}(\vartheta)$ acts on system (1), then it can be rewritten as follows [34]:

$$\begin{cases} \boldsymbol{x}(\vartheta+1) & = \boldsymbol{A}\boldsymbol{x}(\vartheta) + \boldsymbol{A_d}\boldsymbol{x}(\vartheta - d(\vartheta)) + \boldsymbol{B}u(\vartheta) + \boldsymbol{F}\bar{\boldsymbol{w}}(\vartheta), \\ \boldsymbol{y}(\boldsymbol{\vartheta}) & = \boldsymbol{D}\boldsymbol{x}(\vartheta) + \boldsymbol{E}\bar{\boldsymbol{w}}(\vartheta), \end{cases} \tag{2}$$

where, $\boldsymbol{x}(\vartheta) \in \mathbb{R}^n$ is the system state vector, $u(\vartheta) \in \mathbb{R}^m$ is the control input. $\bar{\boldsymbol{w}}(\vartheta) \in \mathbb{R}^n$ is external noise signal which belongs to $l_2[0,\infty)$, $y(\vartheta)$ represents output vector of the system. $\boldsymbol{A}, \boldsymbol{A_d}, \boldsymbol{B}, \boldsymbol{F}, \boldsymbol{D},$ and $\boldsymbol{E}$ are known matrices that have appropriate dimensions. $d(\vartheta)$ denotes the time varying delay which is positive integer, d_l and d_h are the lower and upper delay bounds, respectively and $d_l \leq d(\vartheta) \leq d_h$.

This article adopts the logarithmic quantizer $q(\cdot)$ defined as follows to enhance transmission efficiency in communication channels

$$q(\mathfrak{v}) = [q_1(\mathfrak{v}_1), q_2(\mathfrak{v}_2), \cdots, q_r(\mathfrak{v}_{\mathfrak{r}})]^T, \quad \forall \mathfrak{v} \in \mathbb{R}^n, \tag{3}$$

where, $q_j(\cdot)$ $(1 \leq j \leq r)$ denotes the j^{th} quantizer with the quantized density represented as η^i $(0 \leq \eta^i \leq 1)$. This set of quantization levels is given by

$$\Gamma = \left\{ \pm u_i = \eta^{(i)} u_0, i = \pm 1, \pm 2, ... \right\} \cup \{0\}, \ u_0 > 0. \tag{4}$$

Moreover, the j^{th} quantizer can be expressed as:

$$q_j(c) = \begin{cases} u_i, & \frac{1}{1+\alpha_j} u_i < c \leq \frac{1}{1-\alpha_j} u_i, \\ 0, & c = 0, \\ -q_j(-c), & c < 0, \end{cases} \tag{5}$$

with $\alpha_j = ([1-\eta^{(i)}]/[1+\eta^{(i)}])$.

Accordingly, $q_i(c)$ can be represented as

$$q_i(c) = (1 + \Delta_{qj})c, \tag{6}$$

where, $\Delta_{qj} \in [-\alpha_j, \alpha_j)$.

Defining $\Delta_q = diag\left\{\Delta_{qj}\right\}$, the quantization of the state can be expressed as

$$q(c) = (1 + \Delta_q)c, \tag{7}$$

According to definition of Δ_q, by selecting $\hat{\boldsymbol{\Delta}} = diag\{a_1, a_2, \cdots a_r\}$ an uncertain real-valued time-varying matrix $\hat{\Sigma} = \Delta_q \hat{\boldsymbol{\Delta}}^{-1}$ and satisfying $\hat{\Sigma}^T \hat{\Sigma} \leq \boldsymbol{I}$.

In general, there are kinds of quantization in the field. One is logarithmic quantization (5). The other one is well-distributed quantization, which can be expressed as

$$q(\mathfrak{v}) = \begin{cases} 0, & -\frac{1}{2} < \mathfrak{v} < \frac{1}{2}, \\ i, & \frac{2i-1}{2} < \mathfrak{v} < \frac{2i+1}{2}, i = 1, 2, ... \\ -q(-\mathfrak{v}), & \mathfrak{v} \leq -\frac{1}{2}. \end{cases} \tag{8}$$

By comparing (5) and (8), instead of dividing a uniform range of input signal, as is used in uniform quantization, into equal quantization levels/logarithmic divisions, divide the range by step values which are proportional to each level's own size and based on the amplitude of its samples. This approach lowers the errors for small signals, i.e., improves accuracy, and save resources for large signals. Accordingly, a logarithmic quantizer is adopted to enhance the efficiency of communication.

To mitigate the problem of inefficient transmission, an event-triggering mechanism is introduced, which helps to ease bandwidth usage. The sensors then release the latest data at time $\boldsymbol{x}(\vartheta_i)$ and $\boldsymbol{x}(\vartheta_i + j)$ provided that the following triggering condition is fulfilled:

$$\beta_s^T(\vartheta)\boldsymbol{\Omega}\beta_s(\vartheta) > \rho\, \boldsymbol{x}^T(\vartheta_i)\boldsymbol{\Omega}\boldsymbol{x}(\vartheta_i), \tag{9}$$

where, $\beta_s^T = \boldsymbol{x}(\vartheta_i + j) - \boldsymbol{x}(\vartheta_i)$, $\rho \in [-1, 1)$ represents proportional threshold, and $\Omega > 0$ is a positive definite matrix.

If condition (9) holds, the event detector is able to transmit the most recent data. The subsequent event-triggered instant can then be expressed as follows:

$$\boldsymbol{x}(\vartheta_i + 1) = \boldsymbol{x}(\vartheta_i) + \min_{j \geq 1} \left\{ j | \beta_s^T(\vartheta)\boldsymbol{\Omega}\beta_s(\vartheta) > \rho \boldsymbol{x}^T(\vartheta_i)\boldsymbol{\Omega}\boldsymbol{x}(\vartheta_i) \right\}. \tag{10}$$

Here, $\boldsymbol{x}(\vartheta_i)$ represent the present transmission instant, while $\boldsymbol{x}(\vartheta_i + 1)$ indicates the upcoming instant.

Owing to the influence of the practical ETC, the subsequent sampled state $x(\vartheta_i + j)$ $(j \in [0, \vartheta_{i+1} - \vartheta_i - 1])$ will not be transmitted at the instant $\vartheta_i + j$. In addition, $\boldsymbol{x}(\vartheta_i + 1)$ satisfies

$$\beta_s^T(\vartheta)\boldsymbol{\Omega}\beta_s(\vartheta) \leq \rho \boldsymbol{x}^T(\vartheta_i)\boldsymbol{\Omega}\boldsymbol{x}(\vartheta_i). \tag{11}$$

It is assumed that the system is influenced solely by network-induced delays. Let h_i represent the delay associated with i^{th} transmission, where $h_i \in [h_m, h_M]$. h_m and h_M are the positive constants. Clearly, $j^* \in \mathbb{N}^+$ holds.

The following subsets are defined over the given time interval $[\vartheta_i + h_i, \vartheta_{i+1} + h_{i+1})$

$$\begin{cases} h_i \leq h(\vartheta) \leq \bar{h}, & \vartheta \in [\vartheta_i + h_i, \vartheta_i + h_M + 1), \\ h_i \leq h_M \leq h(\vartheta) \leq \bar{h}, & \vartheta \in \cup_{j=1}^{j^*-1} [\vartheta_i + h_M + j, \vartheta_i + h_M + j + 1), \\ h_i \leq h_M \leq h(\vartheta) \leq \bar{h}, & \vartheta \in [\vartheta_i + h_M + j^*, \vartheta + h_{i+1}). \end{cases} \tag{12}$$

Here $j = 1, 2, 3, ..., j^* - 1$. Based on (12), one has

$$[\vartheta_i + h_i, \quad \vartheta_{i+1} + h_{i+1}) = \begin{cases} [\vartheta_i + h_i, \vartheta_i + h_M + 1) \\ \cup\{\cup_{j=1}^{j^*-1}[\vartheta_i + h_M + j, \vartheta_i + h_M + j + 1)\} \\ \cup[\vartheta_i + h_M + j^*, \vartheta + h_{i+1}). \end{cases} \tag{13}$$

The following function is defined as

$$h(\vartheta) = \begin{cases} \vartheta - \vartheta_i, & \vartheta \in [\vartheta_i + h_i, \vartheta_i + h_M + 1), \\ \vartheta - \vartheta_i - j, & \vartheta \in \cup\{\cup_{j=1}^{j^*-1}[\vartheta_i + h_M + j, \vartheta_i + h_M + j + 1)\}, \\ \vartheta - \vartheta_i - j^*, & \vartheta \in \cup[\vartheta_i + h_M + j^*, \vartheta + h_{i+1}), \end{cases} \tag{14}$$

and

$$\beta_s(\vartheta) = \begin{cases} 0 & \vartheta \in [\vartheta_i + h_i, \vartheta_i + h_M + 1), \\ \boldsymbol{x}(\vartheta_i) - \boldsymbol{x}(\vartheta_i + j), & \vartheta \in \cup\{\cup_{j=1}^{j^*-1}[\vartheta_i + h_M + j, \vartheta_i + h_M + j + 1)\}, \\ \boldsymbol{x}(\vartheta_i) - \boldsymbol{x}(\vartheta_i + j^*), & \vartheta \in \cup[\vartheta_i + h_M + j^*, \vartheta + h_{i+1}). \end{cases} \tag{15}$$

According to (14), the expression becomes

$$0 \leq h_m \leq h_i \leq h(\vartheta) \leq \bar{h}, \tag{16}$$

where, $\bar{h} = 1 + h_M$.

Therefore, based on the ETCs (9) and (15), it follows that for $\vartheta \in [\vartheta + h_i, \vartheta_{i+1} + h_{i+1})$

$$\boldsymbol{\beta_s}^T(\vartheta)\boldsymbol{\Omega}\boldsymbol{\beta_s}(\vartheta) \leq \rho[\boldsymbol{x}(\vartheta - h(\vartheta) + \boldsymbol{\beta_s}(\vartheta)]^T\boldsymbol{\Omega}[(\boldsymbol{x}(\vartheta - h(\vartheta) + \boldsymbol{\beta_s}(\vartheta))]. \tag{17}$$

Because the controller's signal is susceptible to appropriation, leakage, or malicious damage, it may result in failure when considering the opening of the network account. In this case, the random deception attack is assumed to be directed at the controller. Generally, a nonlinear function $\boldsymbol{h}(\boldsymbol{x}(\vartheta))$ that is related to $\boldsymbol{x}(\vartheta)$ can be used to describe the attack signal. Next, a new controller design model that takes into account cyberattacks and quantized event-triggering is introduced as

$$\begin{aligned} u(\vartheta) &= \boldsymbol{K}[q\boldsymbol{x}(\vartheta_i) + \eta(\vartheta)\boldsymbol{h}(\boldsymbol{x}(\vartheta))], \\ &= \boldsymbol{K}(\boldsymbol{I} + \Delta_q)[\boldsymbol{x}(\vartheta - h(\vartheta)) + \boldsymbol{\beta_s}(\vartheta)] + \eta(\vartheta)\boldsymbol{K}\boldsymbol{h}(\boldsymbol{x}(\vartheta)). \end{aligned} \tag{18}$$

Let $\eta(\vartheta) \in \{0, 1\}$ be a random variable governed by a Bernoulli distribution, which characterizes the probability of the cyberattack occurrence. Moreover, the nonlinear function $\boldsymbol{h}(\boldsymbol{x}(\vartheta))$ is assumed to satisfy the following Lipschitz conditions:

$$\|h(x) - h(y)\| \leq \|\Lambda(x - y)\|, \tag{19}$$

where Λ denotes a constant matrix that serves as the upper bound of $h(\cdot)$.

Remark 1 The cyberattack is represented by a nonlinear function, the control input in (18) can be expressed in two possible forms. When $\eta(\vartheta) = 0$, the input becomes $u(\vartheta) = \boldsymbol{K}(I + \Delta_q)[\boldsymbol{x}(\vartheta - h(\vartheta)) + \boldsymbol{\beta_s}(\vartheta)]$ meaning that no attack occurs during the information transmission. Conversely, when $\eta(\vartheta) = 1$, the input is given by $u(\vartheta) = \boldsymbol{K}(I + \Delta_q)[\boldsymbol{x}(\vartheta - h(\vartheta)) + \boldsymbol{\beta_s}(\vartheta)] + \boldsymbol{K}\boldsymbol{h}(\boldsymbol{x}(\vartheta))$, which reflects the situation where the controller is influenced by malicious attack signals. The stochastic nature of this process is characterized as follows:

$$Prob\,\{\eta(\vartheta) = 1\} = \bar{\eta}, \qquad Prob\,\{\eta(\vartheta) = 0\} = 1 - \bar{\eta}, \tag{20}$$

where $\bar{\eta}$ denotes a predefined parameter.

Substituting equation (18) into (1), the system can be reformulated as follows.

$$\begin{cases} \boldsymbol{x}(\vartheta + 1) = \boldsymbol{A}\boldsymbol{x}(\vartheta) + \boldsymbol{A_d}\boldsymbol{x}(\vartheta - d(\vartheta)) + \boldsymbol{B}\boldsymbol{K}(\boldsymbol{I} + \Delta_q)[\boldsymbol{x}(\vartheta - h(\vartheta)) \\ \qquad\qquad + \boldsymbol{\beta_s}(\vartheta)] + \eta(\vartheta)\boldsymbol{K}\boldsymbol{h}(\boldsymbol{x}(\vartheta)). \end{cases} \tag{21}$$

Definition 1 [21] System (2) is said to be passive. If there a scalar $\alpha > 0$ such that for all $\bar{\boldsymbol{w}}(\vartheta) \in [0, \infty)$, the following inequality holds under zero initial condition:

$$2\sum_{i=0}^{\vartheta} y^T(i)\boldsymbol{w}(i) \geq -\alpha \sum_{i=0}^{\vartheta} \boldsymbol{w}^T(i)\boldsymbol{w}(i), \qquad \forall\vartheta > 0. \tag{22}$$

Lemma 1 [14] *For a given matrix $\boldsymbol{R} > 0$ satisfying $\boldsymbol{R}^T = \boldsymbol{R} > 0$, integers $q_2 \geq q_1$, any discrete-time variable $x : [q_1, q_2] \to \mathbb{R}^n$, the inequality holds as follows:*

$$\begin{aligned} (q_2 - q_1)\sum_{i=q_1}^{q_2} \eta^T(i)\boldsymbol{R}\eta(i) &\geq \begin{bmatrix} v_1 \\ v_2 \end{bmatrix}^T \begin{bmatrix} \boldsymbol{R} & 0 \\ 0 & \acute{\rho}(q_1, q_2)3\boldsymbol{R} \end{bmatrix} \begin{bmatrix} v_1 \\ v_2 \end{bmatrix}, \\ &\geq \begin{bmatrix} v_1 \\ v_2 \end{bmatrix}^T \begin{bmatrix} \boldsymbol{R} & 0 \\ 0 & \acute{\rho}(q_1, q_2)3\boldsymbol{R} \end{bmatrix} \begin{bmatrix} v_1 \\ v_2 \end{bmatrix}, \end{aligned}$$

where, $\eta(k) = z(k+1) - z(k)$, $v_1 = z(q_2) - z(q_1)$, $v_2 = z(q_2) + z(q_1) - 2\sum_{i=q_1}^{b}(z_i/[q_2 - q_1 + 1])$, $\acute{\rho}(q_1, q_2) = ([q_2 - q_1 + 1/b - q_1 - 1])$ for $q_2 - q_1 \neq 1$, and $\acute{\rho}(q_1, q_2) = 1$ for $q_2 - q_1 = 1$.

Lemma 2 [14] *For a real value $\tilde{\beta} \in (0, 1)$, a matrix $\boldsymbol{R}$ satisfying $\boldsymbol{R}^T = \boldsymbol{R} > 0$, and any matrix S satisfying $\begin{bmatrix} \boldsymbol{R} & \boldsymbol{S} \\ * & \boldsymbol{R} \end{bmatrix} \geq 0$, the matrix inequality holds as follows:*

$$\begin{bmatrix} \frac{1}{\tilde{\beta}}\boldsymbol{R} & 0 \\ 0 & \frac{1}{1-\tilde{\beta}}\boldsymbol{R} \end{bmatrix} \geq \begin{bmatrix} \boldsymbol{R} & \boldsymbol{S} \\ * & \boldsymbol{R} \end{bmatrix}.$$

Lemma 3 [28] *For any real matrices σ_1, σ_2, and σ_3 with appropriate dimensions and $\sigma_3^T\sigma_3 \leq I$, it follows that*

$$\sigma_1\sigma_3\sigma_2 + \sigma_2^T\sigma_3^T\sigma_1^T \leq \eta_a\sigma_1\sigma_1^T + \eta_a^{-1}\sigma_2^T\sigma_2, \quad \forall\eta_a > 0.$$

3 Main Results

This section presents an improved stability criterion for system (21). Using an augmented LKF, a sufficient condition is established to examine asymptotic stability in delayed DTSs. For simplicity,

$$\begin{aligned}
\Gamma(\vartheta) &= \left[\boldsymbol{x}^T(\vartheta)\ \textstyle\sum_{s=\vartheta-d_l}^{\vartheta-1}\boldsymbol{x}^T(s)\ \sum_{s=\vartheta-d_h}^{\vartheta-d_l-1}\boldsymbol{x}^T(s)\right]^T,\\
e_k &= [0_{n\times(k-1)n}\ \boldsymbol{I}_{n\times n}\ 0_{n\times(16-k)n}],\ k = 1, ...16. \text{ For example}\\
e_6 &= [0\,0\,0\,0\,0\,\boldsymbol{I}\ \underbrace{0\,0\,0}_{10 \text{ times}}\,],\\
\Delta V_n(\vartheta) &= V_n(\vartheta+1) - V_n(\vartheta), n = 1, 2, 3, ...\\
\boldsymbol{\chi}(\vartheta) &= [\boldsymbol{x}(\vartheta), \boldsymbol{x}(\vartheta+1), \boldsymbol{x}(\vartheta-d_l), \boldsymbol{x}(\vartheta-d_h), \boldsymbol{x}(\vartheta-d(\vartheta)), \boldsymbol{x}(\vartheta-h_m),\\
&\quad \boldsymbol{x}(\vartheta-\bar{h}), \boldsymbol{x}(\vartheta-h(\vartheta)), \frac{1}{d_l+1}\sum_{\beta=\vartheta-d_l}^{\vartheta}\boldsymbol{x}(\beta), \frac{1}{d_h-d(\vartheta)+1}\sum_{\beta=\vartheta-d_h}^{\vartheta-d(\vartheta)}\boldsymbol{x}(\beta),\\
&\quad \frac{1}{d(\vartheta)-d_l+1}\sum_{\beta=\vartheta-d(\vartheta)}^{\vartheta-d_l}\boldsymbol{x}(\beta), \frac{1}{h_m+1}\sum_{\beta=\vartheta-h_m}^{\vartheta}\boldsymbol{x}(\beta), \frac{1}{\bar{h}-h(\vartheta)+1}\\
&\quad \times\sum_{\beta=\vartheta-\bar{h}}^{\vartheta-h(v)}\boldsymbol{x}(\beta), \frac{1}{h(\vartheta)-h_m+1}\sum_{\beta=\vartheta-h(\vartheta)}^{\vartheta-h_m}\boldsymbol{x}(\beta), \boldsymbol{\beta_s}(\vartheta), \boldsymbol{h}(\boldsymbol{x}(\vartheta))],\\
\boldsymbol{\chi}_1(\vartheta) &= [\boldsymbol{\chi}(\vartheta), \bar{\boldsymbol{w}}(\vartheta)],\\
\mathfrak{Y}_1 &= \begin{bmatrix} \boldsymbol{x}(\vartheta+1)\\ d_1\sum_{\beta=\vartheta-d_l}^{\vartheta}\boldsymbol{x}(\beta) - \boldsymbol{x}(\vartheta-d_l)\\ d_3\sum_{\beta=\vartheta-d(\vartheta)}^{\vartheta-d_l}\boldsymbol{x}(\beta) - \boldsymbol{x}(\vartheta-d(\vartheta)) + d_3\sum_{\vartheta-d(\vartheta)}^{\vartheta-d_l}\boldsymbol{x}(\beta) - \boldsymbol{x}(\vartheta-d_h)\end{bmatrix},\\
\mathfrak{Y}_2 &= \begin{bmatrix} \boldsymbol{x}(\vartheta)\\ d_1\sum_{\beta=\vartheta-d_l}^{\vartheta}\boldsymbol{x}(\beta) - \boldsymbol{x}(\vartheta)\\ d_3\sum_{\beta=\vartheta-d(\vartheta)}^{\vartheta-d_l}\boldsymbol{x}(\beta) - \boldsymbol{x}(\vartheta-d_l) + d_2\sum_{\beta=\vartheta-d_h}^{\vartheta-d(\vartheta)}\boldsymbol{x}(\beta) - \boldsymbol{x}(\vartheta-d(\vartheta))\end{bmatrix},\\
d_1 &= d_l+1, d_2 = d_h - d(\vartheta) + 1, d_3 = d(\vartheta) - d_l + 1, h_{12} = \bar{h} - h_m,\\
d_{lh} &= d_h - d_l,\ \mathcal{R}_1 = diag\{\boldsymbol{R_1}, 3\boldsymbol{R_1}\},\ \mathcal{R}_2 = diag\{\boldsymbol{R_2}, 3\boldsymbol{R_2}\},\\
\mathcal{R}_4 &= diag\{\boldsymbol{R_4}, 3\boldsymbol{R_4}\},\ \mathcal{R}_5 = diag\{\boldsymbol{R_5}, 3\boldsymbol{R_5}\}.
\end{aligned}$$

Theorem 1 *For given scalars $d_h > d_l > 0, \bar{h} > h_m > 0, \rho > 0, \bar{\eta}, \epsilon_1 > 0, \epsilon_2 > 0$ and control gain matrix $\boldsymbol{K}$, the system (21) is asymptotically stable if there exist* *positive symmetric matrices* $\boldsymbol{P}$, $\boldsymbol{Q_1}$, $\boldsymbol{Q_2}$, $\boldsymbol{Q_3}$, $\boldsymbol{Q_4}$, $\boldsymbol{R_1}$, $\boldsymbol{R_2}$, $\boldsymbol{R_4}$, $\boldsymbol{R_5}$ *and any matrices* $\boldsymbol{G_1}$, $\boldsymbol{G_2}$, $\boldsymbol{T}$, $\boldsymbol{S}$, *matrix* $\boldsymbol{\Omega}$ *of compatible dimensions, such that the following inequalities are satisfied:*

$$\Xi = \begin{bmatrix} \mathfrak{T} & \epsilon_1 G_1^T \boldsymbol{BK} & \epsilon_2 G_2^T \boldsymbol{BK} \\ * & -\epsilon_1 \boldsymbol{I} & 0 \\ * & * & -\epsilon_2 \boldsymbol{I} \end{bmatrix} < 0, \tag{23}$$

$$\begin{bmatrix} \mathcal{R}_2 & \boldsymbol{T} \\ * & \mathcal{R}_2 \end{bmatrix} \geq 0, \tag{24}$$

$$\begin{bmatrix} \mathcal{R}_5 & \boldsymbol{S} \\ * & \mathcal{R}_5 \end{bmatrix} \geq 0, \tag{25}$$

where

$$\mathfrak{T} = \sum_{i=1}^{8} \mathfrak{T}_i,$$

$$\begin{aligned}
\mathfrak{T}_1 =& \boldsymbol{e_2^T P e_2} - d_3 \boldsymbol{e_{11}^T P e_4} + \boldsymbol{e_5^T P e_4} - d_2 \boldsymbol{e_{10}^T P e_4} - \boldsymbol{e_4^T P} d_3 \boldsymbol{e_{11}} + \boldsymbol{e_4^T P e_5} \\
& - \boldsymbol{e_4^T P} d_2 \boldsymbol{e_{10}} + \boldsymbol{e_4^T P e_4} - \boldsymbol{e_1^T P e_1} + d_3 \boldsymbol{e_{11}^T P e_3} + \boldsymbol{e_3^T P} d_3 \boldsymbol{e_{11}} - \boldsymbol{e_3^T P e_3} \\
& + \boldsymbol{e_3^T P} d_2 \boldsymbol{e_{10}} - \boldsymbol{e_3^T P e_5} + d_2 \boldsymbol{e_{10}^T P e_3} - \boldsymbol{e_5^T P e_3}, \\
\mathfrak{T}_2 =& \boldsymbol{e_1^T Q_1 e_1} + \boldsymbol{e_3^T Q_2 e_3} - \boldsymbol{e_3^T Q_1 e_3} - \boldsymbol{e_4^T Q_2 e_4}, \mathfrak{T}_3 = \boldsymbol{e_1^T Q_3 e_1} - \boldsymbol{e_6^T Q_3 e_6}, \\
\mathfrak{T}_4 =& \boldsymbol{e_1^T Q_4 e_1} - \boldsymbol{e_7^T Q_4 e_7}, \mathfrak{T}_5 = d_l [\boldsymbol{e_2^T R_1 e_2} - 2\boldsymbol{e_2^T R_1 e_1} + \boldsymbol{e_1^T R_1 e_1}] \\
& + d_{lh} [\boldsymbol{e_2^T R_2 e_2} - 2\boldsymbol{e_2^T R_2 e_1} + \boldsymbol{e_1^T R_2 e_1}] + \theta_1 + \theta_2, \\
\mathfrak{T}_6 =& h_m^2 [\boldsymbol{e_2^T R_4 e_2} - 2\boldsymbol{e_2^T R_4 e_1} + \boldsymbol{e_1^T R_4 e_1}] + \theta_3, \\
\mathfrak{T}_7 =& h_{12}^2 [\boldsymbol{e_2^T R_5 e_2} - 2\boldsymbol{e_2^T R_5 e_1} + \boldsymbol{e_1^T R_5 e_1}] + \theta_4, \\
\mathfrak{T}_8 =& 2\boldsymbol{G_1^T} [\boldsymbol{e_1^T e_2} + \boldsymbol{e_1^T A e_1} + \boldsymbol{e_1^T A_d e_5} + \boldsymbol{e_1^T BK e_8} + \boldsymbol{e_1^T BK e_{15}} \\
& + \boldsymbol{e_1^T} \eta(\vartheta) \boldsymbol{BK e_{16}}] + 2G_2^T [\boldsymbol{e_2^T e_2} + \boldsymbol{e_2^T A e_1} + \boldsymbol{e_2^T A_d e_5} + \boldsymbol{e_2^T BK e_8} \\
& + \boldsymbol{e_2^T BK e_{15}} + \boldsymbol{e_2^T} \eta(\vartheta) \boldsymbol{BK e_{16}}] + \epsilon_1^{-1} \boldsymbol{e_8^T} \hat{\boldsymbol{\Delta}}^T \hat{\Delta} \boldsymbol{e_8} + \epsilon_2^{-1} \boldsymbol{e_{15}^T} \hat{\boldsymbol{\Delta}}^T \hat{\Delta} \boldsymbol{e_{15}}.
\end{aligned}$$

Proof Consider the following LKF:

$$V(x(\vartheta)) = \sum_{n=1}^{7} V_n(\vartheta), \tag{26}$$

$$
\begin{aligned}
V_1(x(\vartheta)) &= \boldsymbol{\Gamma}^T(\vartheta)\boldsymbol{P}\boldsymbol{\Gamma}(\vartheta),\\
V_2(x(\vartheta)) &= \sum_{\beta=\vartheta-d_l}^{\vartheta-1} \boldsymbol{x}^{\boldsymbol{T}}(\beta)\boldsymbol{Q_1x}(\beta) + \sum_{\beta=\vartheta-d_h}^{\vartheta-d_l-1} \boldsymbol{x}^{\boldsymbol{T}}(\beta)\boldsymbol{Q_2x}(\beta),\\
V_3(x(\vartheta)) &= \sum_{\beta=\vartheta-h_m}^{\vartheta-1} \boldsymbol{x}^{\boldsymbol{T}}(\beta)\boldsymbol{Q_3x}(\beta),\\
V_4(x(\vartheta)) &= \sum_{\beta=\vartheta-\bar{h}}^{\vartheta-1} \boldsymbol{x}^{\boldsymbol{T}}(\beta)\boldsymbol{Q_4x}(\beta),\\
V_5(x(\vartheta)) &= d_l \sum_{\beta=-d_l}^{-1}\sum_{\gamma=\vartheta+\beta}^{\vartheta-1} \Delta\boldsymbol{x}^{\boldsymbol{T}}(\gamma)\boldsymbol{R_1}\Delta x(\gamma) + d_{lh}\sum_{\beta=-d_h}^{-1-d_l}\sum_{\gamma=\vartheta+\beta}^{\vartheta-1} \Delta x^T(\gamma)\boldsymbol{R_2}\Delta x(\gamma),\\
V_6(x(\vartheta)) &= h_m \sum_{\gamma=-h_m}^{-1}\sum_{\beta=\vartheta+m}^{\vartheta-1} \Delta x^T(\beta)\boldsymbol{R_4}\Delta x(\beta),\\
V_7(x(\vartheta)) &= h_{12} \sum_{\gamma=-\bar{h}}^{-h_m-1}\sum_{\beta=\vartheta+m}^{\vartheta-1} \Delta x^T(\beta)\boldsymbol{R_5}\Delta x(\beta).
\end{aligned}
$$

Subsequently, by determining of $V_n(\vartheta)$ for $n = 0, 1, 2, 3...7$ and applying expectation of these difference, we can get

$$
\Delta V_1(\boldsymbol{x}(\vartheta)) = \mathfrak{Y}_1^T P\mathfrak{Y}_1 - \mathfrak{Y}_2^T\boldsymbol{P}\mathfrak{Y}_2 = \chi^T(\vartheta)\mathfrak{T}_1\chi(\vartheta), \tag{27}
$$

$$
\begin{aligned}
\Delta V_2(\boldsymbol{x}(\vartheta)) =& \boldsymbol{x}^{\boldsymbol{T}}(\vartheta)\boldsymbol{Q_1x}(\vartheta) + \boldsymbol{x}^{\boldsymbol{T}}(\vartheta-d_l)\boldsymbol{Q_2x}(\vartheta-d_l)\\
&- \boldsymbol{x}^{\boldsymbol{T}}(\vartheta-d_l)\boldsymbol{Q_1x}(\vartheta-d_l) - \boldsymbol{x}^{\boldsymbol{T}}(\vartheta-d_h)\boldsymbol{Q_2x}(\vartheta-d_h),\\
=& \chi^T(\vartheta)\mathfrak{T}_2\chi(\vartheta),
\end{aligned} \tag{28}
$$

$$
\Delta V_3(\boldsymbol{x}(\vartheta)) = \boldsymbol{x}^{\boldsymbol{T}}(\vartheta)\boldsymbol{Q_3x}(\vartheta) - \boldsymbol{x}^{\boldsymbol{T}}(\vartheta-h_m)\boldsymbol{Q_3x}(\vartheta-h_m) = \chi^T(\vartheta)\mathfrak{T}_3\chi(\vartheta), \tag{29}
$$

$$
\Delta V_4(\boldsymbol{x}(\vartheta)) = \boldsymbol{x}^{\boldsymbol{T}}(\vartheta)\boldsymbol{Q_4x}(\vartheta) - \boldsymbol{x}^{\boldsymbol{T}}(\vartheta-\bar{h})\boldsymbol{Q_4x}(\vartheta-\bar{h}) = \chi^T(\vartheta)\mathfrak{T}_4\chi(\vartheta), \tag{30}
$$

$$
\Delta V_5(\boldsymbol{x}(\vartheta)) = \begin{cases} d_l\Delta x^T(\vartheta)\boldsymbol{R_1}\Delta x(\vartheta) + d_{lh}\Delta x^T(\vartheta)\boldsymbol{R_2}\Delta x(\vartheta)\\ -d_l\sum_{\beta=\vartheta-d_l}^{\vartheta-1}\Delta x^T(\beta)\boldsymbol{R_1}\Delta x(\beta)\\ -d_{lh}\sum_{\beta=\vartheta-d_h}^{\vartheta-1-d_l}\Delta x^T(\beta)\boldsymbol{R_2}\Delta x(\beta). \end{cases} \tag{31}
$$

By applying Lemma 1 and Lemma 2, the summation terms in (31), we can get

$$
\begin{aligned}
&-d_l\sum_{\beta=\vartheta-d_l}^{\vartheta-1}\Delta x^T(\beta)\boldsymbol{R_1}\Delta x(\beta) \le -\begin{bmatrix}\boldsymbol{e_1}-\boldsymbol{e_3}\\ \boldsymbol{e_1}+\boldsymbol{e_3}-2\boldsymbol{e_9}\end{bmatrix}^T \mathcal{R}_1\begin{bmatrix}\boldsymbol{e_1}-\boldsymbol{e_3}\\ \boldsymbol{e_1}+\boldsymbol{e_3}-2\boldsymbol{e_9}\end{bmatrix} \le \theta_1,\\
&-d_{lh}\sum_{\beta=\vartheta-d_h}^{\vartheta-1-d_l}\Delta x^T(\beta)\boldsymbol{R_2}\Delta x(\beta)
\end{aligned}
$$

$$= \left[-d_{lh} \sum_{\beta=\vartheta-d_h}^{\vartheta-1-d(\vartheta)} \Delta x^T(\beta) \boldsymbol{R_2} \Delta x(\beta) - d_{lh} \sum_{\beta=\vartheta-d(\vartheta)}^{\vartheta-1-d_l} \Delta x^T(\beta) \boldsymbol{R_2} \Delta x(\beta) \right],$$

$$\leq \left[-\frac{d_{lh}}{d_h - d(\vartheta)} \begin{bmatrix} \boldsymbol{e_5} - \boldsymbol{e_4} \\ \boldsymbol{e_5} + \boldsymbol{e_4} - 2\boldsymbol{e_{10}} \end{bmatrix}^T \mathcal{R}_2 \begin{bmatrix} \boldsymbol{e_5} - \boldsymbol{e_4} \\ \boldsymbol{e_5} + \boldsymbol{e_4} - 2\boldsymbol{e_{10}} \end{bmatrix} - \frac{d_{lh}}{d(\vartheta) - d_l} \right.$$

$$\left. \times \begin{bmatrix} \boldsymbol{e_3} - \boldsymbol{e_5} \\ \boldsymbol{e_3} + \boldsymbol{e_5} - 2\boldsymbol{e_{11}} \end{bmatrix} \mathcal{R}_2 \begin{bmatrix} \boldsymbol{e_3} - \boldsymbol{e_5} \\ \boldsymbol{e_3} + \boldsymbol{e_5} - 2\boldsymbol{e_{11}} \end{bmatrix} \right],$$

$$\leq - \begin{bmatrix} \boldsymbol{e_5} - \boldsymbol{e_4} \\ \boldsymbol{e_5} + \boldsymbol{e_4} - 2\boldsymbol{e_{10}} \\ \boldsymbol{e_3} - \boldsymbol{e_5} \\ \boldsymbol{e_3} + \boldsymbol{e_5} - 2\boldsymbol{e_{11}} \end{bmatrix}^T \begin{bmatrix} \mathcal{R}_2 & T \\ * & \mathcal{R}_2 \end{bmatrix} \begin{bmatrix} \boldsymbol{e_5} - \boldsymbol{e_4} \\ \boldsymbol{e_5} + \boldsymbol{e_4} - 2\boldsymbol{e_{10}} \\ \boldsymbol{e_3} - \boldsymbol{e_5} \\ \boldsymbol{e_3} + \boldsymbol{e_5} - 2\boldsymbol{e_{11}} \end{bmatrix} \leq \theta_2,$$

$$\Delta V_5(\boldsymbol{x}(\vartheta)) = \chi^T(\vartheta) \mathfrak{T}_5 \chi(\vartheta), \tag{32}$$

$$\Delta V_6(\boldsymbol{x}(\vartheta)) = h_m^2 \Delta x^T(\vartheta) \boldsymbol{R_4} \Delta x(\vartheta) - h_m \sum_{\beta=\vartheta-h_m}^{\vartheta-1} \Delta x^T(\beta) \boldsymbol{R_4} \Delta x(\beta). \tag{33}$$

By utilizing Lemma 1 and Lemma 2 the summation terms in (33), we can get

$$-h_m \sum_{\gamma=\vartheta-h_m}^{\vartheta-1} \Delta x^T(\beta) \boldsymbol{R_4} \Delta x(\beta)$$

$$\leq - \begin{bmatrix} \boldsymbol{e_1} - \boldsymbol{e_6} \\ \boldsymbol{e_1} + \boldsymbol{e_6} - 2\boldsymbol{e_{12}} \end{bmatrix}^T \mathcal{R}_4 \begin{bmatrix} \boldsymbol{e_1} - \boldsymbol{e_6} \\ \boldsymbol{e_1} + \boldsymbol{e_6} - 2\boldsymbol{e_{12}} \end{bmatrix} \leq \theta_4,$$

$$\Delta V_6(\boldsymbol{x}(\vartheta)) = \chi^T(\vartheta) \mathfrak{T}_6 \chi(\vartheta), \tag{34}$$

$$\Delta V_7(\boldsymbol{x}(\vartheta)) = h_{12}^2 \Delta x^T(\vartheta) \boldsymbol{R_5} \Delta x(\vartheta) - h_{12} \sum_{\beta=\vartheta-\bar{h}}^{\vartheta-h_m-1} \Delta x^T(\beta) \boldsymbol{R_5} \Delta x(\beta). \tag{35}$$

Similarly from Lemma 1 and Lemma 2 the summation terms in (35), we can get

$$-h_{12} \sum_{\beta=\vartheta-\bar{h}}^{\vartheta-h_m-1} \Delta x^T(\beta) \boldsymbol{R_5} \Delta x(\beta)$$

$$= \left[-h_{12} \sum_{\beta=\vartheta-\bar{h}}^{\vartheta-h(\vartheta)-1} \Delta x^T(\beta) \boldsymbol{R_5} \Delta x(\beta) - h_{12} \sum_{\beta=\vartheta-h(\vartheta)}^{\vartheta-h_m-1} \Delta x^T(\beta) \boldsymbol{R_5} \Delta x(\beta) \right],$$

$$\leq - \frac{h_{12}}{\bar{h} - h(\vartheta)} \begin{bmatrix} \boldsymbol{e_8} - \boldsymbol{e_7} \\ \boldsymbol{e_8} + \boldsymbol{e_7} - 2\boldsymbol{e_{13}} \end{bmatrix}^T \mathcal{R}_5 \begin{bmatrix} \boldsymbol{e_8} - \boldsymbol{e_7} \\ \boldsymbol{e_8} + \boldsymbol{e_7} - 2\boldsymbol{e_{13}} \end{bmatrix} - \frac{h_{12}}{h(\vartheta) - h_m}$$

$$\times \begin{bmatrix} \boldsymbol{e_6} - \boldsymbol{e_8} \\ \boldsymbol{e_6} + \boldsymbol{e_8} - 2\boldsymbol{e_{14}} \end{bmatrix}^T \mathcal{R}_5 \begin{bmatrix} \boldsymbol{e_6} - \boldsymbol{e_8} \\ \boldsymbol{e_6} + \boldsymbol{e_8} - 2\boldsymbol{e_{14}} \end{bmatrix},$$

$$\leq \begin{bmatrix} \boldsymbol{e_8} - \boldsymbol{e_7} \\ \boldsymbol{e_8} + \boldsymbol{e_7} - 2\boldsymbol{e_{13}} \\ \boldsymbol{e_6} - \boldsymbol{e_8} \\ \boldsymbol{e_6} + \boldsymbol{e_8} - 2\boldsymbol{e_{14}} \end{bmatrix}^T \begin{bmatrix} \mathcal{R}_5 & \boldsymbol{S} \\ * & \mathcal{R}_5 \end{bmatrix} \begin{bmatrix} \boldsymbol{e_8} - \boldsymbol{e_7} \\ \boldsymbol{e_8} + \boldsymbol{e_7} - 2\boldsymbol{e_{13}} \\ \boldsymbol{e_6} - \boldsymbol{e_8} \\ \boldsymbol{e_6} + \boldsymbol{e_8} - 2\boldsymbol{e_{14}} \end{bmatrix} \leq \theta_5,$$

$$\Delta_7(\boldsymbol{x}(\vartheta)) = \chi^T(\vartheta)\mathfrak{T}_7\chi(\vartheta). \tag{36}$$

Moreover, for any compatible matrices $\boldsymbol{G_1}$ and $\boldsymbol{G_2}$, the following relation can be derived from system (1)

$$\begin{aligned} 0 = &Sym[\boldsymbol{x}^T(\vartheta)\boldsymbol{G_1} + \boldsymbol{x}^T(\vartheta+1)\boldsymbol{G_2}][-\boldsymbol{x}(\vartheta+1) + \boldsymbol{A}\boldsymbol{x}(\vartheta) + \boldsymbol{A_d}\boldsymbol{x}(\vartheta - d(\vartheta)) \\ &+ \boldsymbol{BK}(\boldsymbol{I} + \Delta_q)[\boldsymbol{x}(\vartheta - h(\vartheta)) + \beta_s(\vartheta)] + \eta(\vartheta)\boldsymbol{BKh}(x(\vartheta))], \\ 0 = &\chi^T(\vartheta)\mathfrak{T}_8\chi(\vartheta), \end{aligned} \tag{37}$$

for the positive scalars ϵ_1 and ϵ_2, the following inequalities are directly obtained

$$\begin{aligned} 2\boldsymbol{x}^T(\vartheta)\boldsymbol{G}_1^T\boldsymbol{K}\Delta_q\boldsymbol{x}(\vartheta - h(\vartheta)) \leq &\epsilon_1\boldsymbol{x}^T(\vartheta)\boldsymbol{G}_1^T\boldsymbol{BKK}^T\boldsymbol{B}^T\boldsymbol{G_1}\boldsymbol{x}(\vartheta) \\ &+ \epsilon_1^{-1}\boldsymbol{x}^T(\vartheta - h(\vartheta))\hat{\Delta}^T\hat{\Delta}\boldsymbol{x}(\vartheta - h(\vartheta)), \end{aligned} \tag{38}$$

$$\begin{aligned} 2\boldsymbol{x}^T(\vartheta+1)\boldsymbol{G}_2^T\boldsymbol{K}\Delta_q\beta_s(\vartheta) \leq &\epsilon_2\boldsymbol{x}^T(\vartheta+1)\boldsymbol{G}_2^T\boldsymbol{BKK}^T\boldsymbol{B}^T\boldsymbol{G_2}\boldsymbol{x}(\vartheta+1) \\ &+ \epsilon_2^{-1}\beta_s(\vartheta)\hat{\Delta}^T\hat{\Delta}\beta_s(\vartheta)). \end{aligned} \tag{39}$$

Thus, $\Delta V(\vartheta)$ is expressed as

$$\begin{aligned} &\Delta V(\vartheta) \\ &\quad \leq \chi^T(\vartheta)[\mathfrak{T} + \epsilon_1\boldsymbol{e_1}\boldsymbol{G}_1^T\boldsymbol{BKK}^T\boldsymbol{B}^T\boldsymbol{G_1}\boldsymbol{e}_1^T + \epsilon_2\boldsymbol{e_2}\boldsymbol{G}_2^T\boldsymbol{BKK}^T\boldsymbol{B}^T\boldsymbol{G_2}\boldsymbol{e}_2^T]\chi(\vartheta). \end{aligned} \tag{40}$$

Using the Schur complement on (40), we get $\Delta V(\vartheta) < 0$, which means that the system (21) is asymptotically stable. □

Remark 2 In this work, a simple LKF is developed without introducing complicated LKF-like triple-summation terms. The lemmas applied to proposed method can provide some better results for Theorem 1. Furthermore, Theorem 2 is motivated by Theorem 1, and we design a resilient ETC to achieve the asymptotic stability of the closed-loop system in the presence of quantization and deception attacks.

3.1 Resilient Event-Triggered Controller Design:

It is noted that the modelled controller's arguments in earlier literature works may have been extremely delicate or sensitive to different variations in the feedback gain. The subsequent control concept is being used to frame a gain for feedback control. The ETC framework for DTS will be covered in the ensuing Theorem 2. Additionally, the control gain can be represented as $\boldsymbol{K} + \Delta\boldsymbol{K}$. Here,

$$\Delta\boldsymbol{K} = \boldsymbol{H}\delta\boldsymbol{J}, \tag{41}$$

where, $\boldsymbol{H}$ and $\boldsymbol{J}$ are known matrices and δ is unknown matrix, that unknown matrix satisfies $\delta^T\delta = I$. Consider the system operating with a resilient ETC strategy

$$\begin{cases} \boldsymbol{x}(\vartheta+1) = \boldsymbol{A}\boldsymbol{x}(\vartheta) + \boldsymbol{A_d}\boldsymbol{x}(\vartheta - d(\vartheta)) + \boldsymbol{B}u(\vartheta), \\ \quad u(\vartheta) = \boldsymbol{K}(\boldsymbol{I}+\Delta_q)[\boldsymbol{x}(\vartheta - h(\vartheta) + \beta_s(\vartheta)] + \eta(\vartheta)\boldsymbol{K}\boldsymbol{h}(x(\vartheta)). \end{cases} \tag{42}$$

Theorem 2 *For these scalars d_l, d_h, $\bar{h}$, h_m, ϵ, ϵ_1, ϵ_2, $\bar{\eta}$, ρ, η_a, η_b and the system (42)is asymptotically stable and with the help of the event triggered controller (17), if there exist positive definite symmetric matrices $\bar{P}$, $\bar{Q}_1$, $\bar{Q}_2$, $\bar{Q}_3$, $\bar{Q}_4$, $\bar{R}_1$, $\bar{R}_2$, $\bar{R}_4$, $\bar{R}_5$, $\bar{\Omega}$, K, G, and any matrices $\bar{T}$, $\bar{S}$, X satisfy the following LMI condition:*

$$\begin{bmatrix} \hat{\Xi} & \hat{\mathbb{M}}_1 & \eta_a\hat{\mathbb{N}}_{\boldsymbol{1}}^{\boldsymbol{T}} & \hat{\mathbb{M}}_2 & \eta_b\hat{\mathbb{N}}_{\boldsymbol{2}}^{\boldsymbol{T}} \\ * & -\eta_a\boldsymbol{I} & 0 & 0 & 0 \\ * & * & -\eta_a\boldsymbol{I} & 0 & 0 \\ * & * & * & -\eta_b\boldsymbol{I} & 0 \\ * & * & * & * & -\eta_b\boldsymbol{I} \end{bmatrix} < 0, \tag{43}$$

$$\begin{bmatrix} \bar{\boldsymbol{\mathcal{R}}}_{\boldsymbol{2}} & \bar{\boldsymbol{T}} \\ * & \bar{\boldsymbol{\mathcal{R}}}_{\boldsymbol{2}} \end{bmatrix} \geq 0, \tag{44}$$

$$\begin{bmatrix} \bar{\boldsymbol{\mathcal{R}}}_{\boldsymbol{5}} & \bar{\boldsymbol{S}} \\ * & \bar{\boldsymbol{\mathcal{R}}}_{\boldsymbol{5}} \end{bmatrix} \geq 0, \tag{45}$$

where,

$$\hat{\Xi}_{18\times18} = \begin{bmatrix} \boldsymbol{\Xi_1} & \boldsymbol{\Xi_2} \\ * & \boldsymbol{\Xi_3} \end{bmatrix}, \ \boldsymbol{\Xi_1} = \boldsymbol{l}_{9\times9}, \ \ \boldsymbol{\Xi_2} = \boldsymbol{L}_{9\times9}, \ \ \boldsymbol{\Xi_3} = \boldsymbol{H}_{9\times9},$$

$$\begin{aligned}
\boldsymbol{l_{11}} =& - \bar{\boldsymbol{P}} + \bar{\boldsymbol{Q}}_{\boldsymbol{1}} + \bar{\boldsymbol{Q}}_{\boldsymbol{3}} + \bar{\boldsymbol{Q}}_{\boldsymbol{4}} + d_l^2\bar{\boldsymbol{R}}_1 + d_{lh}^2\bar{\boldsymbol{R}}_{\boldsymbol{2}} - \bar{\boldsymbol{R}}_{\boldsymbol{1}} - 3\bar{\boldsymbol{R}}_1 + h_m^2\bar{\boldsymbol{R}}_{\boldsymbol{4}} - \bar{\boldsymbol{R}}_{\boldsymbol{4}} \\
& - 3\bar{\boldsymbol{R}}_{\boldsymbol{4}} + h_{12}^2\bar{\boldsymbol{R}}_{\boldsymbol{5}} + 2\boldsymbol{A}\boldsymbol{G}, \ \boldsymbol{l_{12}} = -d_{lh}^2\bar{\boldsymbol{R}}_{\boldsymbol{2}} - d_l^2\bar{\boldsymbol{R}}_{\boldsymbol{1}} - h_m^2\bar{\boldsymbol{R}}_{\boldsymbol{4}} - h_{12}^2\bar{\boldsymbol{R}}_{\boldsymbol{5}} - \boldsymbol{G} \\
& + \epsilon\boldsymbol{A}\boldsymbol{G}, \boldsymbol{l_{13}} = -3\bar{\boldsymbol{R}}_{\boldsymbol{1}} + \bar{\boldsymbol{R}}_{\boldsymbol{1}}, \ \boldsymbol{l_{15}} = \boldsymbol{A_d}\boldsymbol{G}, \boldsymbol{l_{16}} = \bar{\boldsymbol{R}}_{\boldsymbol{4}} - 3\bar{\boldsymbol{R}}_{\boldsymbol{4}}, \boldsymbol{l_{18}} = \boldsymbol{B}\boldsymbol{X}, \\
\boldsymbol{l_{19}} =& 6\bar{\boldsymbol{R}}_{\boldsymbol{1}}, \boldsymbol{l_{22}} = \bar{\boldsymbol{P}} + d_l^2\bar{\boldsymbol{R}}_{\boldsymbol{1}} + d_{lh}^2\bar{\boldsymbol{R}}_{\boldsymbol{2}} + h_m^2\bar{\boldsymbol{R}}_{\boldsymbol{4}} + h_{12}^2\bar{\boldsymbol{R}}_{\boldsymbol{5}} - 2\epsilon\boldsymbol{G}, \boldsymbol{l_{25}} = \epsilon\boldsymbol{A_d}\boldsymbol{G}, \\
\boldsymbol{l_{28}} =& \epsilon\boldsymbol{B}\boldsymbol{X}, \boldsymbol{l_{33}} = -\bar{\boldsymbol{P}} + \bar{\boldsymbol{Q}}_{\boldsymbol{2}} - \bar{\boldsymbol{Q}}_{\boldsymbol{1}} - \bar{\boldsymbol{R}}_{\boldsymbol{1}} - 3\bar{\boldsymbol{R}}_{\boldsymbol{1}} - \bar{\boldsymbol{R}}_{\boldsymbol{2}} - 3\bar{\boldsymbol{R}}_{\boldsymbol{2}}, \\
\boldsymbol{l_{34}} =& -\bar{\boldsymbol{T}} + \bar{\boldsymbol{T}} - \bar{\boldsymbol{T}} - \bar{\boldsymbol{T}}, \boldsymbol{l_{35}} = -\bar{\boldsymbol{P}} - \bar{\boldsymbol{T}} - \bar{\boldsymbol{T}} - \bar{\boldsymbol{T}} - \bar{\boldsymbol{T}} + \bar{\boldsymbol{R}}_{\boldsymbol{2}} - 3\bar{\boldsymbol{R}}_{\boldsymbol{2}}, \\
\boldsymbol{l_{39}} =& 6\bar{\boldsymbol{R}}_{\boldsymbol{1}}, l_{44} = \bar{\boldsymbol{P}} - \bar{\boldsymbol{Q}}_{\boldsymbol{2}} - \bar{\boldsymbol{R}}_{\boldsymbol{2}} - 3\bar{\boldsymbol{R}}_{\boldsymbol{2}}, \boldsymbol{l_{45}} = \bar{\boldsymbol{P}} + \bar{\boldsymbol{R}}_{\boldsymbol{2}} - 3\bar{\boldsymbol{R}}_{\boldsymbol{2}} - \bar{\boldsymbol{T}} + \bar{\boldsymbol{T}} - \bar{\boldsymbol{T}} \\
& - \bar{\boldsymbol{T}}, \boldsymbol{l_{55}} = \bar{\boldsymbol{R}}_{\boldsymbol{2}} + \bar{\boldsymbol{T}} - \bar{\boldsymbol{T}} - 3\bar{\boldsymbol{R}}_{\boldsymbol{2}} + \bar{\boldsymbol{T}} + \bar{\boldsymbol{T}} + \bar{\boldsymbol{T}} - \bar{\boldsymbol{T}} - \bar{\boldsymbol{R}}_{\boldsymbol{2}} - \bar{\boldsymbol{T}} - \bar{\boldsymbol{T}} \\
& - 3\bar{\boldsymbol{R}}_{\boldsymbol{2}}, \boldsymbol{l_{66}} = -\bar{\boldsymbol{Q}}_{\boldsymbol{3}} - \bar{\boldsymbol{R}}_{\boldsymbol{4}} - 3\bar{\boldsymbol{R}}_{\boldsymbol{4}} - \bar{\boldsymbol{R}}_{\boldsymbol{5}} - 3\bar{\boldsymbol{R}}_{\boldsymbol{5}}, \boldsymbol{l_{67}} = \bar{\boldsymbol{S}} + \bar{\boldsymbol{S}} - \bar{\boldsymbol{S}} - \bar{\boldsymbol{S}}, \\
\boldsymbol{l_{68}} =& \bar{\boldsymbol{R}}_{\boldsymbol{5}} - 3\bar{\boldsymbol{R}}_{\boldsymbol{5}} - \bar{\boldsymbol{S}} - \bar{\boldsymbol{S}} - \bar{\boldsymbol{S}} - \bar{\boldsymbol{S}}, \boldsymbol{l_{77}} = -\bar{\boldsymbol{Q}}_{\boldsymbol{4}} - \bar{\boldsymbol{R}}_{\boldsymbol{5}} - 3\bar{\boldsymbol{R}}_{\boldsymbol{5}}, \boldsymbol{l_{78}} = -\bar{\boldsymbol{S}} + \bar{\boldsymbol{S}} \\
& + \bar{\boldsymbol{S}} - \bar{\boldsymbol{S}} + \bar{\boldsymbol{R}}_{\boldsymbol{5}} - 3\bar{\boldsymbol{R}}_{\boldsymbol{5}}, \boldsymbol{l_{88}} = -\bar{\boldsymbol{R}}_{\boldsymbol{5}} + \bar{\boldsymbol{S}} + \bar{\boldsymbol{S}} - 3\bar{\boldsymbol{R}}_{\boldsymbol{5}} - \bar{\boldsymbol{S}} - \bar{\boldsymbol{S}} + \bar{\boldsymbol{S}} - \bar{\boldsymbol{S}} \\
& - \bar{\boldsymbol{R}}_{\boldsymbol{5}} + \bar{\boldsymbol{S}} - \bar{\boldsymbol{S}} - 3\bar{\boldsymbol{R}}_{\boldsymbol{5}} + \rho\bar{\boldsymbol{\Omega}}, \boldsymbol{l_{99}} = -12\bar{\boldsymbol{R}}_{\boldsymbol{1}},
\end{aligned}$$

$$
\begin{aligned}
\boldsymbol{L_{13}} =& 6\bar{\boldsymbol{R}}_{\boldsymbol{4}},\ \boldsymbol{L_{16}} = \boldsymbol{BX},\ \boldsymbol{L_{17}} = \bar{\eta}\boldsymbol{BX},\ \boldsymbol{L_{18}} = \epsilon_1\boldsymbol{BX},\ \boldsymbol{L_{26}} = \epsilon\boldsymbol{BX},\\
\boldsymbol{L_{27}} =& \epsilon\bar{\eta}\boldsymbol{BX},\ \boldsymbol{L_{29}} = \epsilon_2\boldsymbol{BX},\ \boldsymbol{L_{31}} = \bar{\boldsymbol{P}} + 2\bar{\boldsymbol{T}} + 2\bar{\boldsymbol{T}}, \boldsymbol{L_{32}} = \bar{\boldsymbol{P}} + 6\bar{\boldsymbol{R}}_{\boldsymbol{2}},\\
\boldsymbol{L_{41}} =& -\bar{\boldsymbol{P}} + 6\bar{\boldsymbol{R}}_{\boldsymbol{2}},\ L_{42} = -\bar{\boldsymbol{P}} + 2\bar{\boldsymbol{T}} + 2\bar{\boldsymbol{T}}, \boldsymbol{L_{51}} = 6\bar{\boldsymbol{R}}_{\boldsymbol{2}} - 2\bar{\boldsymbol{T}} + 2\bar{\boldsymbol{T}}\\
\boldsymbol{L_{52}} =& 6\bar{\boldsymbol{R}}_{\boldsymbol{2}} + 2\bar{\boldsymbol{T}} + 2\bar{\boldsymbol{T}}, \boldsymbol{L_{63}} = 6\bar{\boldsymbol{R}}_{\boldsymbol{4}}, \boldsymbol{L_{64}} = 2\bar{\boldsymbol{S}} + 2\bar{\boldsymbol{S}}, \boldsymbol{L_{65}} = 6\bar{\boldsymbol{R}}_{\boldsymbol{5}},\\
\boldsymbol{L_{74}} =& 6\bar{\boldsymbol{R}}_{\boldsymbol{5}}, \boldsymbol{L_{75}} = -2\bar{\boldsymbol{S}} + 2\bar{\boldsymbol{S}}, \boldsymbol{L_{84}} = -2\bar{\boldsymbol{S}} + 2\bar{\boldsymbol{S}} + 6\bar{\boldsymbol{R}}_{\boldsymbol{5}}, \boldsymbol{L_{85}} = -2\bar{\boldsymbol{S}} + 2\bar{\boldsymbol{S}}\\
&+ 6\bar{\boldsymbol{R}}_{\boldsymbol{5}}, \boldsymbol{L_{86}} = \bar{\boldsymbol{\Omega}}\rho, \boldsymbol{L_{87}} = \boldsymbol{G}^{\boldsymbol{T}}\boldsymbol{\Lambda}^{\boldsymbol{T}}, \boldsymbol{L_{88}} = \boldsymbol{G}^{\boldsymbol{T}}\hat{\boldsymbol{\Delta}}^{\boldsymbol{T}}, \boldsymbol{L_{89}} = \boldsymbol{G}^{\boldsymbol{T}}\hat{\boldsymbol{\Delta}}^{\boldsymbol{T}},\\
\boldsymbol{H_{11}} =& -12\bar{\boldsymbol{R}}_{\boldsymbol{2}}, \boldsymbol{H_{12}} = -4\bar{\boldsymbol{T}}, \boldsymbol{H_{22}} = -12\bar{\boldsymbol{R}}_{\boldsymbol{2}}, \boldsymbol{H_{33}} = -12\bar{\boldsymbol{R}}_{\boldsymbol{4}}, \boldsymbol{H_{44}} = -12\bar{\boldsymbol{R}}_{\boldsymbol{5}},\\
\boldsymbol{H_{45}} =& -4\boldsymbol{S}, \boldsymbol{H_{55}} = -12\bar{\boldsymbol{R}}_{\boldsymbol{5}}, \boldsymbol{H_{66}} = \rho\bar{\boldsymbol{\Omega}} - \bar{\boldsymbol{\Omega}}, \boldsymbol{H_{77}} = -\boldsymbol{I}, \boldsymbol{H_{88}} = -\epsilon_1\boldsymbol{I},\\
\boldsymbol{H_{99}} =& -\epsilon_2\boldsymbol{I}.
\end{aligned}
$$

Furthermore, the required resilient event-triggered control gain can be derived by $\boldsymbol{K} = \boldsymbol{X}\boldsymbol{G}^{-\boldsymbol{1}}$

Proof To reformulate the inequality (23) by $\boldsymbol{K} = \boldsymbol{K} + \boldsymbol{\Delta K}$, we obtain following result,

$$
\boldsymbol{\Xi} + \mathbb{M}_{\boldsymbol{1}}\delta\mathbb{N}_{\boldsymbol{1}} + \mathbb{N}_{\boldsymbol{1}}^{\boldsymbol{T}}\delta^T\mathbb{M}_{\boldsymbol{1}}^{\boldsymbol{T}} + \mathbb{M}_{\boldsymbol{2}}\delta\mathbb{N}_{\boldsymbol{2}} + \mathbb{N}_{\boldsymbol{2}}^{\boldsymbol{T}}\delta^T\mathbb{M}_{\boldsymbol{2}}^{\boldsymbol{T}}, \tag{46}
$$

where

$$
\begin{aligned}
\mathbb{M}_{\boldsymbol{1}} &= [\underbrace{0...0}_{7\,times}\ \boldsymbol{BH},\ \underbrace{0...0}_{6\,times}, \boldsymbol{BH}, \boldsymbol{BH}\bar{\eta}, \boldsymbol{BH}, 0]^T, \mathbb{N}_{\boldsymbol{1}} = [\boldsymbol{G}_{\boldsymbol{1}}^{\boldsymbol{T}}\boldsymbol{J},\ \underbrace{0...0}_{17\,times}],\\
\mathbb{M}_{\boldsymbol{2}} &= [\underbrace{0...0}_{7\,times}, \boldsymbol{BH}\ \underbrace{0...0}_{6\,times}, \boldsymbol{BH}, \boldsymbol{BH}\bar{\eta}, 0, \boldsymbol{BH}]^T, \mathbb{N}_{\boldsymbol{2}} = [0, \boldsymbol{G}_{\boldsymbol{2}}^{\boldsymbol{T}}\boldsymbol{J},\ \underbrace{0...0}_{16\,times}].
\end{aligned}
$$

Moreover, equation (46) together with Lemma 3 implies the scalars $\eta_a, \eta_b > 0$, satisfying

$$
\boldsymbol{\Xi} + \eta_a^{-1}\mathbb{M}_{\boldsymbol{1}}\mathbb{M}_{\boldsymbol{1}}^{\boldsymbol{T}} + \eta_a\mathbb{N}_{\boldsymbol{1}}^{\boldsymbol{T}}\mathbb{N}_{\boldsymbol{1}} + \eta_b^{-1}\mathbb{M}_{\boldsymbol{2}}\mathbb{M}_{\boldsymbol{2}}^{\boldsymbol{T}} + \eta_b\mathbb{N}_{\boldsymbol{2}}^{\boldsymbol{T}}\mathbb{N}_{\boldsymbol{2}}, \tag{47}
$$

then, using the Schur complement, it is easy to see that

$$
\begin{bmatrix}
\boldsymbol{\Xi} & \mathbb{M}_{\boldsymbol{1}} & \eta_a\mathbb{N}_{\boldsymbol{1}}^{\boldsymbol{T}} & \mathbb{M}_{\boldsymbol{2}} & \eta_b\mathbb{N}_{\boldsymbol{2}}^{\boldsymbol{T}}\\
* & -\eta_a\boldsymbol{I} & 0 & 0 & 0\\
* & * & -\eta_a\boldsymbol{I} & 0 & 0\\
* & * & * & -\eta_b\boldsymbol{I} & 0\\
* & * & * & * & -\eta_b\boldsymbol{I}
\end{bmatrix}, \tag{48}
$$

the remaining proof can be established by employing a similar procedure to that used in Theorem 1. Define

$$
\begin{cases}
\boldsymbol{G_1} = \boldsymbol{G}^{-\boldsymbol{1}}, \boldsymbol{G_2} = \epsilon\boldsymbol{G}^{-\boldsymbol{1}}, \boldsymbol{X} = \boldsymbol{KG}, \bar{\boldsymbol{P}} = \boldsymbol{G}^{\boldsymbol{T}}\boldsymbol{PG}, \bar{\boldsymbol{Q}}_{\boldsymbol{1}} = \boldsymbol{G}^{\boldsymbol{T}}\boldsymbol{Q_1G},\\
\bar{\boldsymbol{Q}}_{\boldsymbol{2}} = \boldsymbol{G}^{\boldsymbol{T}}\boldsymbol{Q_2G}, \bar{\boldsymbol{Q}}_{\boldsymbol{3}} = \boldsymbol{G}^{\boldsymbol{T}}\boldsymbol{Q_3G}, \bar{\boldsymbol{Q}}_{\boldsymbol{4}} = \boldsymbol{G}^{\boldsymbol{T}}\boldsymbol{Q_4G}, \bar{\boldsymbol{R}}_{\boldsymbol{1}} = \boldsymbol{G}^{\boldsymbol{T}}\boldsymbol{R_1G},\\
\bar{\boldsymbol{R}}_{\boldsymbol{2}} = \boldsymbol{G}^{\boldsymbol{T}}\boldsymbol{R_2G}, \bar{\boldsymbol{R}}_{\boldsymbol{4}} = \boldsymbol{G}^{\boldsymbol{T}}\boldsymbol{R_4G}, \bar{\boldsymbol{R}}_{\boldsymbol{5}} = \boldsymbol{G}^{\boldsymbol{T}}\boldsymbol{R_5G},\ \bar{\boldsymbol{\Omega}} = \boldsymbol{G}^{\boldsymbol{T}}\boldsymbol{\Omega G},\\
\bar{\boldsymbol{T}} = \boldsymbol{G}^{\boldsymbol{T}}\boldsymbol{TG},\ \bar{\boldsymbol{S}} = \boldsymbol{G}^{\boldsymbol{T}}\boldsymbol{SG}.
\end{cases} \tag{49}
$$

Condition (43) follows from (48) by apply the congruence transformation with respect to the diagonal matrix $diag\left\{\underbrace{\boldsymbol{G},\boldsymbol{G},\boldsymbol{G}}_{16\,times},\boldsymbol{I},\boldsymbol{I},\boldsymbol{I},\boldsymbol{I},\boldsymbol{I},\boldsymbol{I}\right\}$. □

Remark 1 re3Resilient control strategies have been proposed for nonlinear discrete-time state-delay systems and singular networked systems with random packet losses, where LMI-based conditions are derived to guarantee stability and robustness against uncertainties [17, 28]. In contrast, the resilient event-triggered control (RETC) with the passivity approach is developed in this paper. Generally, the RETC presents better dynamic performance of the closed-loop system and reduces the amount of controller updates and lessing the network communication than the other controller as shown in the numerical example section. The result in Theorem 3 fills the gap on the RETC of DTS under passivity disturbance.

3.2 Resilient Passivity Event-Triggered Controller Design:

The system is investigated in the context of a resilient passivity event-triggered control.

$$\begin{cases} \boldsymbol{x}(\vartheta+1)=\boldsymbol{A}\boldsymbol{x}(\vartheta)+\boldsymbol{A_d}\boldsymbol{x}(\vartheta-d(\vartheta))+\boldsymbol{B}u(\vartheta)+\boldsymbol{F}\bar{\boldsymbol{w}}(\vartheta),\\ \quad u(\vartheta)=\boldsymbol{K}(I+\Delta_q)[\boldsymbol{x}(\vartheta-h(\vartheta))+\boldsymbol{\beta_x}(\vartheta)]+\eta(\vartheta)\boldsymbol{K}\boldsymbol{h}(x(\vartheta)),\\ \quad \boldsymbol{y}(\boldsymbol{\vartheta})=\boldsymbol{D}\boldsymbol{x}(\vartheta)+\boldsymbol{E}\bar{\boldsymbol{w}}(\vartheta). \end{cases} \tag{50}$$

Theorem 3 *For these scalars $d_l, d_h, \bar{h}, h_m, , \epsilon, \epsilon_1, \epsilon_2, \bar{\eta}, \rho, \alpha, \eta_a, \eta_b$ and the system (50) is passive with event-triggered controller (17) if there exist positive symmetric matrices $\bar{\boldsymbol{P}}, \bar{\boldsymbol{Q}}_1, \bar{\boldsymbol{Q}}_2, \bar{\boldsymbol{Q}}_3, \bar{\boldsymbol{Q}}_4, \bar{\boldsymbol{R}}_1, \bar{\boldsymbol{R}}_2, \bar{\boldsymbol{R}}_4, \bar{\boldsymbol{R}}_5, \bar{\boldsymbol{\Omega}}, \boldsymbol{K}, \boldsymbol{G}$ and any matrices $\bar{\boldsymbol{T}}, \bar{\boldsymbol{S}}, \boldsymbol{X}$ satisfy the following LMI condition*

$$\Theta=\begin{bmatrix} \hat{\mathcal{T}} & \hat{\mathbb{M}}_1 & \eta_a\hat{\mathbb{N}}_1^T & \hat{\mathbb{M}}_2 & \eta_b\hat{\mathbb{N}}_2^T\\ * & -\eta_a\boldsymbol{I} & 0 & 0 & 0\\ * & * & -\eta_a\boldsymbol{I} & 0 & 0\\ * & * & * & -\eta_b\boldsymbol{I} & 0\\ * & * & * & * & -\eta_b\boldsymbol{I} \end{bmatrix}<0, \tag{51}$$

$$\begin{bmatrix} \bar{\mathcal{R}}_2 & \bar{\boldsymbol{T}}\\ * & \bar{\mathcal{R}}_2 \end{bmatrix}\geq 0, \tag{52}$$

$$\begin{bmatrix} \bar{\mathcal{R}}_5 & \bar{\boldsymbol{S}}\\ * & \bar{\mathcal{R}}_5 \end{bmatrix}\geq 0, \tag{53}$$

where,

$$\hat{\mathcal{T}}=\begin{bmatrix} \mathcal{T}_1 & \mathcal{T}_2\\ * & \mathcal{T}_3 \end{bmatrix},\ \mathcal{T}_1=\boldsymbol{\mathcal{M}}_{9\times 9},\ \mathcal{T}_2=\boldsymbol{\mathcal{N}}_{9\times 10},\ \mathcal{T}_3=\boldsymbol{\mathcal{O}}_{10\times 10},$$

$$
\begin{aligned}
\mathcal{M}_{11} =& -\bar{P}+\bar{Q}_1+\bar{Q}_3+\bar{Q}_4+d_l^2\boldsymbol{R_1}+d_{lh}^2\bar{\boldsymbol{R}}_2-\bar{\boldsymbol{R}}_1-3\bar{\boldsymbol{R}}_1+h_m^2\bar{\boldsymbol{R}}_4\\
&-\bar{\boldsymbol{R}}_4-3\bar{\boldsymbol{R}}_4+h_{12}^2\bar{\boldsymbol{R}}_5+2\boldsymbol{AG},\ \mathcal{M}_{12}=-d_{lh}^2\bar{\boldsymbol{R}}_2-d_l^2\bar{\boldsymbol{R}}_1-h_m^2\bar{\boldsymbol{R}}_4\\
&-h_{12}^2\bar{\boldsymbol{R}}_5-\boldsymbol{G}+\epsilon\boldsymbol{AG},\ \mathcal{M}_{13}=-3\bar{\boldsymbol{R}}_1+\bar{\boldsymbol{R}}_1,\ \boldsymbol{\mathcal{M}_{15}}=\boldsymbol{A_dG},\\
\mathcal{M}_{16} =&\bar{\boldsymbol{R}}_4-3\bar{\boldsymbol{R}}_4,\ \boldsymbol{\mathcal{M}_{18}}=\boldsymbol{BX},\ \boldsymbol{\mathcal{M}_{19}}=6\bar{\boldsymbol{R}}_1,\ \boldsymbol{\mathcal{M}_{22}}=\bar{\boldsymbol{P}}+d_l^2\bar{\boldsymbol{R}}_1+d_{lh}^2\bar{\boldsymbol{R}}_2\\
&+h_m^2\bar{\boldsymbol{R}}_4+h_{12}^2\bar{\boldsymbol{R}}_5-2\epsilon\boldsymbol{G},\ \boldsymbol{\mathcal{M}_{25}}=\epsilon\boldsymbol{A_dG},\ \boldsymbol{\mathcal{M}_{28}}=\epsilon\boldsymbol{BX},\\
\mathcal{M}_{33} =& -\bar{\boldsymbol{P}}+\bar{\boldsymbol{Q}}_2-\bar{\boldsymbol{Q}}_1-\bar{\boldsymbol{R}}_1-3\bar{\boldsymbol{R}}_1-\bar{\boldsymbol{R}}_2-3\bar{\boldsymbol{R}}_2,\ \boldsymbol{\mathcal{M}_{34}}=-\bar{\boldsymbol{T}}+\bar{\boldsymbol{T}}-\bar{\boldsymbol{T}}-\bar{\boldsymbol{T}},\\
\mathcal{M}_{35} =& -\bar{\boldsymbol{P}}-\bar{\boldsymbol{T}}-\bar{\boldsymbol{T}}-\bar{\boldsymbol{T}}-\bar{\boldsymbol{T}}+\bar{\boldsymbol{R}}_2-3\bar{\boldsymbol{R}}_2,\ \boldsymbol{\mathcal{M}_{39}}=6\bar{\boldsymbol{R}}_1,\ \boldsymbol{\mathcal{M}_{44}}=\bar{\boldsymbol{P}}-\bar{\boldsymbol{Q}}_2\\
&-\bar{\boldsymbol{R}}_2-3\bar{\boldsymbol{R}}_2,\ \boldsymbol{\mathcal{M}_{45}}=\bar{\boldsymbol{P}}+\bar{\boldsymbol{R}}_2-3\bar{\boldsymbol{R}}_2-\bar{\boldsymbol{T}}+\bar{\boldsymbol{T}}-\bar{\boldsymbol{T}}-\bar{\boldsymbol{T}},\ \boldsymbol{\mathcal{M}_{55}}=-\bar{\boldsymbol{R}}_2\\
&+\bar{\boldsymbol{T}}-\bar{\boldsymbol{T}}-3\bar{\boldsymbol{R}}_2+\bar{\boldsymbol{T}}+\bar{\boldsymbol{T}}+\bar{\boldsymbol{T}}-\bar{\boldsymbol{T}}-\bar{\boldsymbol{R}}_2-\bar{\boldsymbol{T}}-\bar{\boldsymbol{T}}-3\bar{\boldsymbol{R}}_2,\\
\mathcal{M}_{66} =& -\bar{\boldsymbol{Q}}_3-\bar{\boldsymbol{R}}_4-3\bar{\boldsymbol{R}}_4-\bar{\boldsymbol{R}}_5-3\bar{\boldsymbol{R}}_5,\ \boldsymbol{\mathcal{M}_{67}}=\bar{\boldsymbol{S}}+\bar{\boldsymbol{S}}-\bar{\boldsymbol{S}}-\bar{\boldsymbol{S}},\ \boldsymbol{\mathcal{M}_{68}}=\bar{\boldsymbol{R}}_5\\
&-3\bar{\boldsymbol{R}}_5-\bar{\boldsymbol{S}}-\bar{\boldsymbol{S}}-\bar{\boldsymbol{S}}-\bar{\boldsymbol{S}},\ \boldsymbol{\mathcal{M}_{77}}=-\bar{\boldsymbol{Q}}_4-\bar{\boldsymbol{R}}_5-3\bar{\boldsymbol{R}}_5,\ \boldsymbol{\mathcal{M}_{78}}=-\bar{\boldsymbol{S}}+\bar{\boldsymbol{S}}\\
&+\bar{\boldsymbol{S}}-\bar{\boldsymbol{S}}+\bar{\boldsymbol{R}}_5-3\bar{\boldsymbol{R}}_5,\ \boldsymbol{\mathcal{M}_{88}}=-\bar{\boldsymbol{R}}_5+\bar{\boldsymbol{S}}+\bar{\boldsymbol{S}}-3\bar{\boldsymbol{R}}_5-\bar{\boldsymbol{S}}-\bar{\boldsymbol{S}}+\bar{\boldsymbol{S}}\\
&-\bar{\boldsymbol{S}}-\bar{\boldsymbol{R}}_5+\bar{\boldsymbol{S}}-\bar{\boldsymbol{S}}-3\bar{\boldsymbol{R}}_5+\rho\bar{\boldsymbol{\Omega}},\ \boldsymbol{\mathcal{M}_{99}}=-12\bar{\boldsymbol{R}}_1,\\
\mathcal{N}_{13} =&6\bar{\boldsymbol{R}}_4,\ \boldsymbol{\mathcal{N}_{16}}=\boldsymbol{BX},\ \boldsymbol{\mathcal{N}_{17}}=\bar{\eta}\boldsymbol{BX},\ \boldsymbol{\mathcal{N}_{18}}=\boldsymbol{F}-\boldsymbol{DG^TF},\\
\mathcal{N}_{19} =&\epsilon_1\boldsymbol{BX},\ \boldsymbol{\mathcal{N}_{26}}=\epsilon\boldsymbol{BX},\ \boldsymbol{\mathcal{N}_{27}}=\epsilon\bar{\eta}\boldsymbol{BX},\ \boldsymbol{\mathcal{N}_{28}}=\epsilon\boldsymbol{F},\ \boldsymbol{\mathcal{N}_{2,10}}=\epsilon_2\boldsymbol{BX},\\
\mathcal{N}_{31} =&\bar{\boldsymbol{P}}+2\bar{\boldsymbol{T}}+2\bar{\boldsymbol{T}},\ \boldsymbol{\mathcal{N}_{32}}=\bar{\boldsymbol{P}}+6\bar{\boldsymbol{R}}_2,\ \boldsymbol{\mathcal{N}_{41}}=-\bar{\boldsymbol{P}}+6\bar{\boldsymbol{R}}_2,\\
\mathcal{N}_{42} =& -\bar{\boldsymbol{P}}+2\bar{\boldsymbol{T}}+2\bar{\boldsymbol{T}},\ \boldsymbol{\mathcal{N}_{51}}=6\bar{\boldsymbol{R}}_2-2\bar{\boldsymbol{T}}+2\bar{\boldsymbol{T}},\ \boldsymbol{\mathcal{N}_{52}}=6\bar{\boldsymbol{R}}_2+2\bar{\boldsymbol{T}}+2\bar{\boldsymbol{T}},\\
\mathcal{N}_{63} =&6\bar{\boldsymbol{R}}_4,\ \boldsymbol{\mathcal{N}_{64}}=2\bar{\boldsymbol{S}}+2\bar{\boldsymbol{S}},\ \boldsymbol{\mathcal{N}_{65}}=6\bar{\boldsymbol{R}}_5,\ \boldsymbol{\mathcal{N}_{74}}=6\bar{\boldsymbol{R}}_5,\ \boldsymbol{\mathcal{N}_{75}}=-2\bar{\boldsymbol{S}}+2\bar{\boldsymbol{S}},\\
\mathcal{N}_{84} =& -2\bar{\boldsymbol{S}}+2\bar{\boldsymbol{S}}+6\bar{\boldsymbol{R}}_5,\ \boldsymbol{\mathcal{N}_{85}}=2\bar{\boldsymbol{S}}+2\bar{\boldsymbol{S}}+6\bar{\boldsymbol{R}}_5,\ \boldsymbol{\mathcal{N}_{86}}=\bar{\boldsymbol{\Omega}}\rho,\ \boldsymbol{\mathcal{N}_{87}}=\boldsymbol{G^T\Lambda^T},\\
\mathcal{N}_{89} =&\boldsymbol{G^T}\hat{\boldsymbol{\Delta}}^{\boldsymbol{T}},\ \boldsymbol{\mathcal{N}_{8,10}}=\boldsymbol{G^T}\hat{\boldsymbol{\Delta}}^{\boldsymbol{T}},\\
\mathcal{O}_{11} =& -12\bar{\boldsymbol{R}}_2,\ \boldsymbol{\mathcal{O}_{12}}=-4\bar{\boldsymbol{T}},\ \boldsymbol{\mathcal{O}_{22}}=-12\bar{\boldsymbol{R}}_2,\\
\mathcal{O}_{33} =& -12\bar{\boldsymbol{R}}_4,\ \boldsymbol{\mathcal{O}_{44}}=-12\bar{\boldsymbol{R}}_5,\ \boldsymbol{\mathcal{O}_{45}}=-4\boldsymbol{S},\ \boldsymbol{\mathcal{O}_{55}}=-12\bar{\boldsymbol{R}}_5,\ \boldsymbol{\mathcal{O}_{66}}=\rho\bar{\boldsymbol{\Omega}}-\bar{\boldsymbol{\Omega}},\\
\mathcal{O}_{77} =& -\boldsymbol{I},\ \boldsymbol{\mathcal{O}_{88}}=-2\boldsymbol{E}-\alpha,\ \boldsymbol{\mathcal{O}_{99}}=-\epsilon_1\boldsymbol{I},\ \boldsymbol{\mathcal{O}_{10,10}}=-\epsilon_2\boldsymbol{I}.
\end{aligned}
$$

In addition, a resilient event-triggered controller gain be achieved by $\boldsymbol{K}=\boldsymbol{XG^{-1}}$.

Proof With the LKF adopted in Theorem 1 and equation (47) of Theorem 2 by applying a similar proof technique, utilizing the Schur complement Lemma, conditions of (49), and applying the congruence transformation with respect to the diagonal matrix $diag\left\{\underbrace{\boldsymbol{G},\boldsymbol{G},\boldsymbol{G}}_{16\,times},\boldsymbol{I},\boldsymbol{I},\boldsymbol{I},\boldsymbol{I},\boldsymbol{I},\boldsymbol{I},\boldsymbol{I}\right\}$. Moreover, we can obtain the following inequality

$$
\Delta V(x(\vartheta))-2\boldsymbol{y}^T(\vartheta)\bar{\boldsymbol{w}}(\vartheta)-\alpha\bar{\boldsymbol{w}}^{\boldsymbol{T}}(\vartheta)\bar{\boldsymbol{w}}(\vartheta)\leq\boldsymbol{\chi_1^T}(\vartheta)\boldsymbol{\Theta}\boldsymbol{\chi_1}(\vartheta), \tag{54}
$$

we get $\boldsymbol{\Theta} < 0$ iff (51) hold.

$$\Delta V(x(\vartheta)) - 2\boldsymbol{y}^T(\vartheta)\bar{\boldsymbol{w}}(\vartheta) - \alpha\bar{\boldsymbol{w}}^{\boldsymbol{T}}(\vartheta)\bar{\boldsymbol{w}}(\vartheta) \leq 0. \tag{55}$$

By summation, the above expression over the interval $[0, \vartheta]$ and taking zero initial conditions, the condition below is derived:

$$2\sum_{i=0}^{\vartheta}\boldsymbol{y}^T(i)\bar{\boldsymbol{w}}(i) \geq \sum_{i=0}^{\vartheta}\Delta V(x(i)) - \alpha\sum_{i=0}^{\vartheta}\bar{\boldsymbol{w}}^T(i)\bar{\boldsymbol{w}}(i), \tag{56}$$

$$=V(\boldsymbol{x}(\vartheta+1)) + V(\boldsymbol{x}(0)) - \alpha\sum_{i=0}^{\vartheta}\bar{\boldsymbol{w}}^{\boldsymbol{T}}(i)\bar{\boldsymbol{w}}(i),$$

$$=V(\boldsymbol{x}(\vartheta+1)) - \alpha\sum_{i=0}^{\vartheta}\bar{\boldsymbol{w}}^{\boldsymbol{T}}(i)\bar{\boldsymbol{w}}(i),$$

$$\geq -\alpha\sum_{i=0}^{\vartheta}\bar{\boldsymbol{w}}^{\boldsymbol{T}}(i)\bar{\boldsymbol{w}}(i). \tag{57}$$

As the above relation meets the Definition of passivity, the system (50) is passive. This concludes the proof. □

Remark 3 Generally, the quantization scheme, Event-triggered control, cyber attack, and passivity disturbance play a main role in this study. It's noted that the authors of [20] investigated the passivity and asymptotic stability of DTS with saturation and disturbance under LKF and LMI. The work presented in [14] explored quantization and ETC of a discrete-time neural network with a deception attack based on synchronization. In [22], the authors are focused on resilient sampled data control, a missing data scenario with the LKF approach, and a sufficient condition in terms of LMI. In [30], the authors proposed an event-triggered transmission scheme, a switching system with a delayed scheme based on a feedback controller and exponential stability. The model considered in the present study is more practical than the above literature [14, 20, 22, 30]. We consider quantization, ETC, passivity disturbance, and stochastic deception attack of a discrete-time system. Due to the many real-life applications, the combined study of passivity and quantization ETC to the system model is more important. The purpose of this study is to establish asymptotic stability conditions of this proposed system by applying the LKF and event-triggered communication scheme. An event will be triggered to update the event-triggered controller when its magnitude reaches the prescribed value. Hence, the comprehensive analysis of the proposed control strategy in the presence of multiple challenges demonstrates the system's relevance and applicability to real-world scenarios.

4 Numerical Examples

In this section, we provide four numerical examples, in that one real application example there. These examples are in order to test the effectiveness and performance of our proposed method. An overview of the resilient control design process is provided as a flowchart in Figure 2.

Example 1 Let us examine the DTS (50) associated with

$$\boldsymbol{A} = \begin{bmatrix} 0.13 & 0.01 \\ -0.22 & 0.04 \end{bmatrix}, \boldsymbol{A_d} = \begin{bmatrix} 0.29 & 0.18 \\ -0.09 & 0.21 \end{bmatrix}, \boldsymbol{D} = \begin{bmatrix} 2.53 & 1.24 \\ -1.53 & 1.54 \end{bmatrix},$$
$$\boldsymbol{B} = \begin{bmatrix} -0.62 & -1.12 \\ 1.23 & 1.3 \end{bmatrix}, \boldsymbol{E} = \begin{bmatrix} 2.25 & 2.29 \\ 2.01 & 1.01 \end{bmatrix}, \boldsymbol{F} = \begin{bmatrix} -0.16 & 0 \\ 0 & -0.11 \end{bmatrix},$$
$$\boldsymbol{I} = \begin{bmatrix} 1 & 0 \\ 0 & 1 \end{bmatrix}, \boldsymbol{H} = \begin{bmatrix} -0.54 & 0 \\ 0 & -0.93 \end{bmatrix}, \boldsymbol{J} = \begin{bmatrix} 0.01 & 0 \\ 0 & -0.03 \end{bmatrix},$$
$$\hat{\boldsymbol{\Delta}}^{\boldsymbol{T}} = \begin{bmatrix} 1 & 0 \\ 0 & 1 \end{bmatrix}, \hat{\boldsymbol{\Lambda}}^{\boldsymbol{T}} = \begin{bmatrix} 0.01 & 0.01 \\ -0.1 & 0.01 \end{bmatrix}.$$

This example determines the largest allowable delay d_h for which the system is strictly asymptotically stable. Using MATLAB LMI toolbox and by taking $d_l = 0.1$, $d_h = 0.3$, $h_m = 0.3$, $\bar{h} = 0.7$, $\alpha = 0.2$, $\rho = 0.6$, $\bar{\eta} = 0.3$ with the above parameters, the LMI conditions of Theorem 3 are examined. For simulation purposes, the exogenous disturbance is assumed to be $\bar{\boldsymbol{w}}(\vartheta) = 0.5\sin(\vartheta)e^{-0.1\vartheta}$. We can obtain the associated control gain matrix together with the triggering parameters as follows

$$\boldsymbol{K} = \begin{bmatrix} 0.0019 & 0.0012 \\ 0.0013 & 0.0014 \end{bmatrix}, \boldsymbol{\Omega} = \begin{bmatrix} 0.0112 & 0.0016 \\ 0.0016 & 0.0054 \end{bmatrix}, \boldsymbol{Q_1} = \begin{bmatrix} 2.0236 & -0.0248 \\ -0.0248 & 0.8609 \end{bmatrix},$$
$$\boldsymbol{Q_2} = \begin{bmatrix} 1.3794 & -0.0520 \\ -0.0520 & 0.5970 \end{bmatrix}, \boldsymbol{R_4} = \begin{bmatrix} 0.0175 & 0.0020 \\ 0.0020 & 0.0089 \end{bmatrix}, \boldsymbol{R_5} = \begin{bmatrix} 0.2489 & 0.0036 \\ 0.0036 & 0.1987 \end{bmatrix}.$$

The figures below depict the simulation outcomes of the DTS (50)when controlled through a quantized event-triggered mechanism scheme by deception attack conditions. The state trajectories $x_1(\vartheta), x_2(\vartheta)$ without deception attacks ($\bar{\eta} = 0$) provided in Figure 3(a) from $x_0 = [-0.5, 2]^T$, the states converge to zero by $\vartheta \approx 180$, faster than with attacks, demonstrating the nominal operating behavior of the ETC scheme. Figure 3(b) presents the state trajectories $x_1(\vartheta)$ and $x_2(\vartheta)$ implemented with ETC during deception attack conditions ($\bar{\eta} = 0.3$). Initial condition starting from $x_0 = [-0.5, 2]^T$, the states converge to zero by $\vartheta \approx 200$ with attack instances 55. The figure highlights the robustness of the system when subjected to deception attacks.

The control inputs $u_1(\vartheta)$ and $u_2(\vartheta)$ without deception attacks ($\bar{\eta} = 0$) illustrated in Figure 4(a) . The inputs converge to zero at $\vartheta \approx 200$, showing steady control behavior with event-triggered updates in the absence of attack disturbances. Figure 4(b) demonstrates the control inputs $u_1(\vartheta)$ and $u_2(\vartheta)$ with deception attacks ($\bar{\eta} = 0.3$). The inputs, beginning from non-zero initial conditions, the states gradually stabilize at

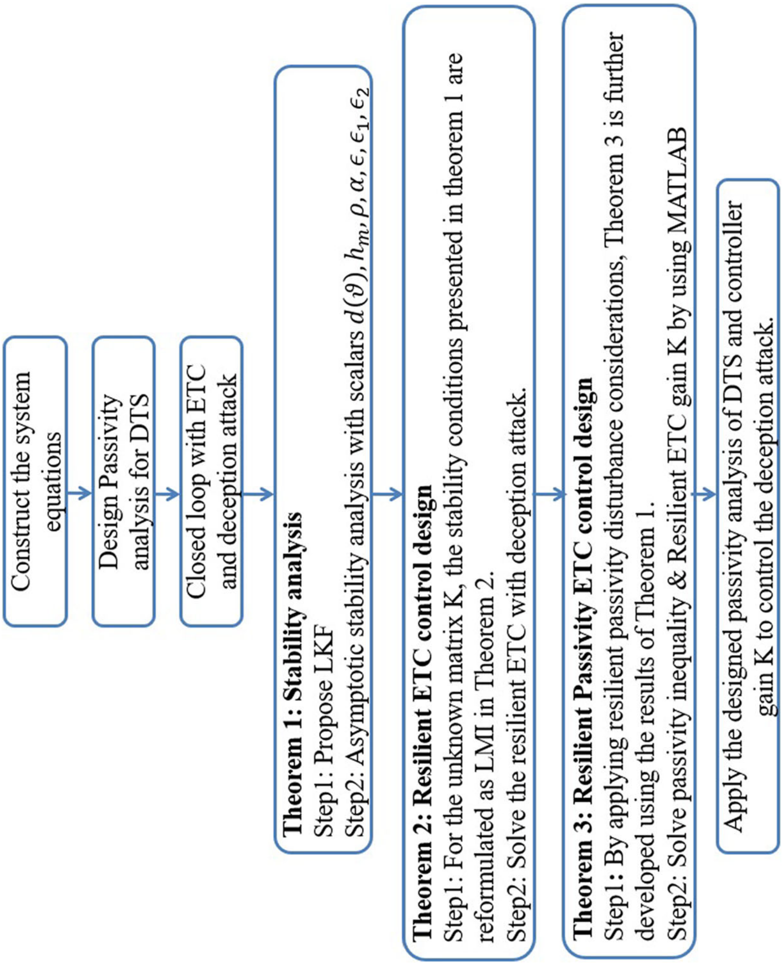

Fig. 2 Resilient Passivity Analysis of DTS with ETC Design Process

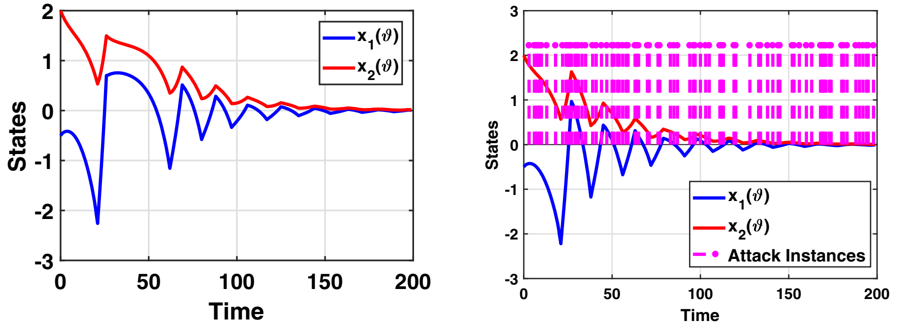

(a) without attacks (b) with attacks

Fig. 3 State Response Curves without and with Attacks for Example 1

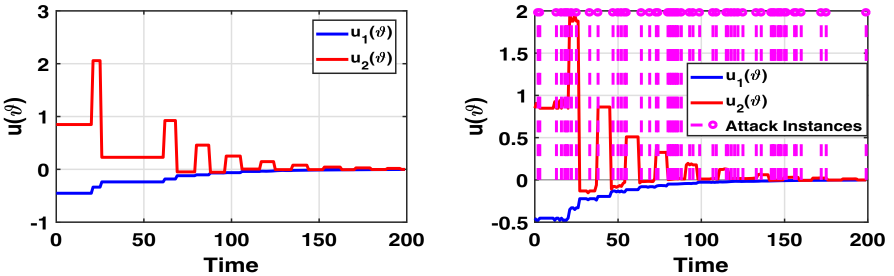

(a) without attack (b) with attacks

Fig. 4 Control Input Responses Without and with Attacks for Example 1

zero with 55 attack instances from $y = 0$ to $y = 2$, examining attack effects on control. Figure 5(a) compares quantized and actual state trajectories $x_1(\vartheta)$ and $x_2(\vartheta)$ with deception attacks ($\bar{\eta} = 0.3$) in two subplots. Actual states (blue, solid) and quantized states (red, dashed) converge to zero, demonstrating effective quantization despite attacks. Figure 5(b) represents the phrase portrait. Figure 6(a) presents the distribution of release intervals for the ETC and Figure 6(b) represents attack intensity.

Figure 7(a) shows the time varying delay $d(\vartheta)$. Graphed as a blue line, the delay varies between 1 and 3 steps randomly, presenting its effect on system dynamics by the robust controller. Figure 7(b) depicted the network-induced delay $h(\vartheta)$. Plotted as a red line, the delay varies between 1 and 2 steps randomly, demonstrating the effects of network dynamics on state propagation in an event-triggered system. Figure 8(a) displays the nonlinear attack function elements $h_1(\vartheta)$, and $h_2(\vartheta)$, with deception attacks ($\bar{\eta} = 0.3$). The elements stabilize to zero, with 71 attack instances from $y = -0.04$ to $y = 0.1$. Figure 8(b) visualizes the Bernoulli distribution $\eta(\vartheta) \in \{0, 1\}$ for deception attacks ($\bar{\eta} = 0.3$). A plot shows 71 attack occurrences, highlighting the random nature of attack events. Figure 9 provides sensitivity analysis of state norm, which depends on various values of ρ, $\bar{\eta}$, Δ_q, and h_M. Figure 10 demonstrates sensitivity analysis of the triggered interval, which also depends on different values of ρ, $\bar{\eta}$, Δ_q, and h_M.

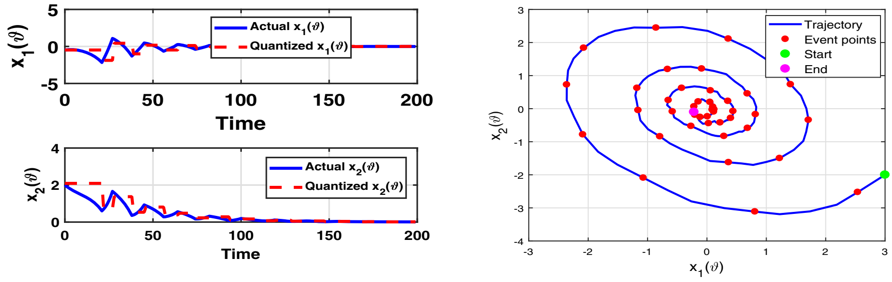

(a) Quantized vs. actual states (b) Phrase portrait

Fig. 5 The Quantized vs. Actual states (with attacks) and Phrase Portrait for Example 1

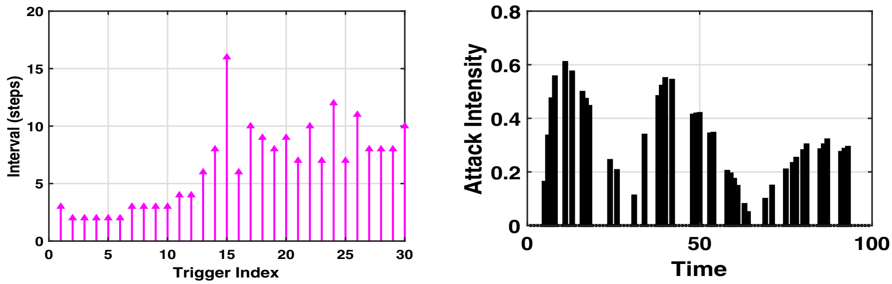

(a) Event-triggered instants (b) Attack intensity

Fig. 6 Event-triggered Release Intervals and Attack Intensity for Example 1

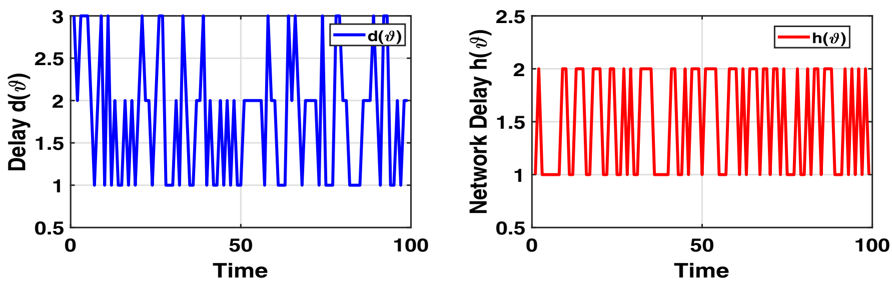

(a) Variable time delay $d(\vartheta)$ (b) Network-induced delay $h(\vartheta)$

Fig. 7 Variation of Variable Time Delay $d(\vartheta)$ and Network-induced Delay $h(\vartheta)$ with Attacks for Example 1

Example 2 Let us examine the DTS (50) associated with

$$\boldsymbol{A} = \begin{bmatrix} 0.2 & 0.30 & 0.05 \\ -0.05 & 0.15 & 0.01 \\ 0.01 & -0.03 & 0.10 \end{bmatrix}, \boldsymbol{A_d} = \begin{bmatrix} 0.02 & 0.01 & 0 \\ 0.6 & -0.03 & 0.6 \\ 0.01 & 0 & 0.02 \end{bmatrix},$$

$$\boldsymbol{B} = \begin{bmatrix} 0.1 & 0.06 & 0.02 \\ -0.02 & 0.01 & -0.01 \\ 0.5 & 0 & 0.03 \end{bmatrix}, \boldsymbol{D} = \begin{bmatrix} 0.3 & 0.1 & 0.01 \\ 0 & 0.4 & 0.5 \\ 0 & 0.02 & 0.3 \end{bmatrix},$$

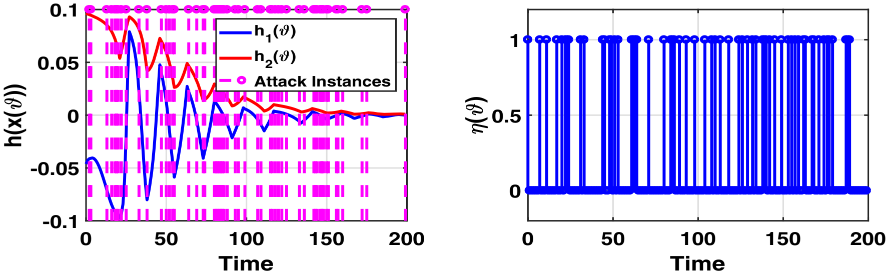

(a) $h(x(\vartheta))$ (b) $\eta(\vartheta)$

Fig. 8 Nonlinear Function $\boldsymbol{h}(\boldsymbol{x}(\vartheta))$ (Attack Occurrences) and Bernoulli Distribution $\eta(\vartheta)$ with Attacks for Example 1

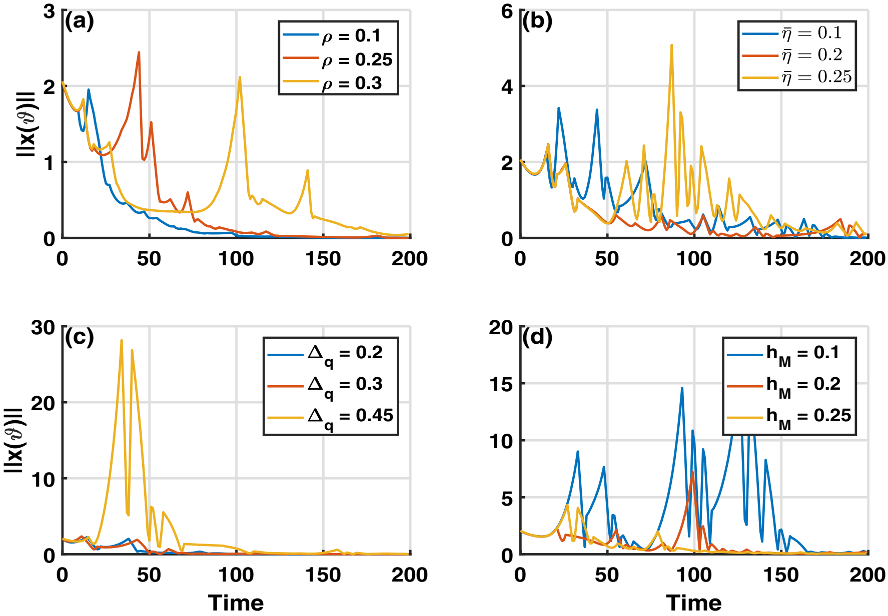

Fig. 9 Sensitivity Analysis of State Norm for Example.1

$$\boldsymbol{E} = \begin{bmatrix} 0.05 & 0.1 & 0 \\ 0.2 & 0.2 & 0.01 \\ 0.1 & 0.15 & 0.08 \end{bmatrix}, \boldsymbol{F} = \begin{bmatrix} 0.1 & 0 & 0 \\ 0 & -0.1 & 0 \\ 0 & 0 & 0.1 \end{bmatrix}, \boldsymbol{H} = \begin{bmatrix} 0.1 & 0 & 0 \\ 0 & 0.3 & 0 \\ 0 & 0 & 0.4 \end{bmatrix},$$

$$\boldsymbol{J} = \begin{bmatrix} 0.1 & 0 & 0 \\ 0 & 0.4 & 0 \\ 0 & 0 & 0.3 \end{bmatrix}, \hat{\boldsymbol{\Delta}}^T = \begin{bmatrix} 1 & 0 & 0 \\ 0 & 1 & 0 \\ 0 & 0 & 1 \end{bmatrix}.$$

To exhibit the effectiveness of the proposed approach, we take $d_l = 0.1$, $d_h = 0.02$, $h_m = 0.1$, $\bar{h} = 0.3$, $\rho = 0.01, \alpha = 0.1$. For the purpose of the simulation, the external disturbance is considered to be $\bar{\boldsymbol{w}}(\vartheta) = [10 * (0.5)^{\vartheta}, -10 * (0.4)^{\vartheta}]^T$.

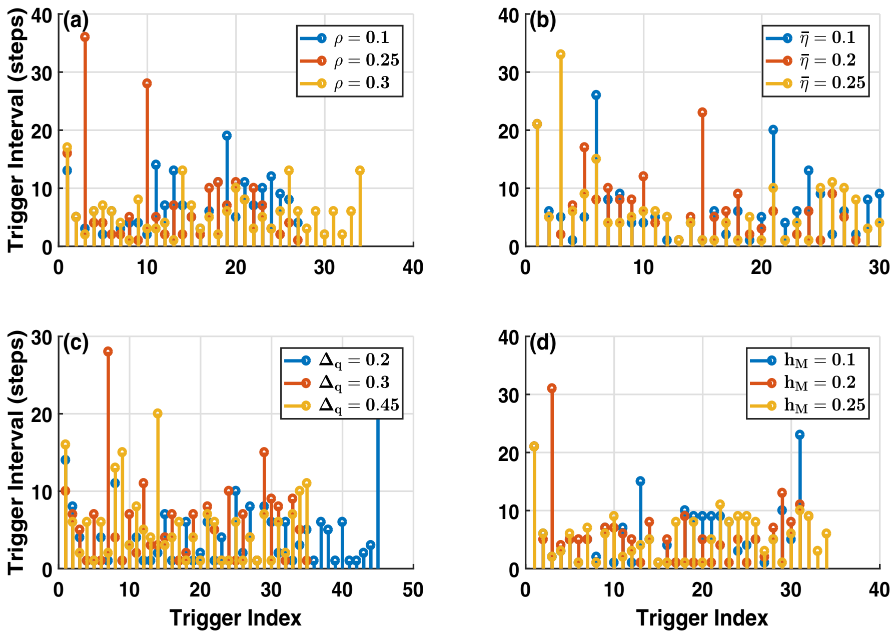

Fig. 10 Sensitivity Analysis of Triggered Interval for Example.1

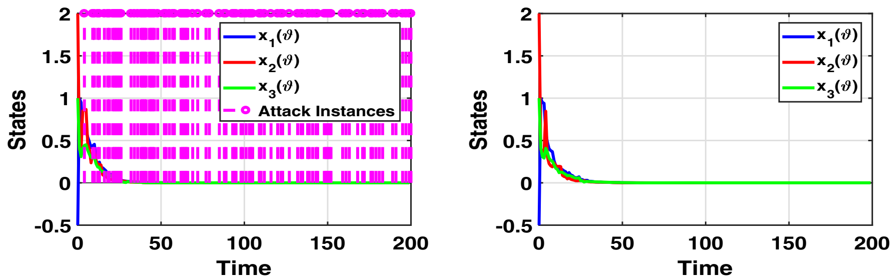

(a) With attacks

(b) Without attack

Fig. 11 State Response Curves with and Without Attacks for Example 2

Solving these conditions by Theorem 3 and using MATLAB toolbox, the ETC gain $\boldsymbol{K}$, and appropriate trigger matrix $\boldsymbol{\Omega}$ from Theorem 3 are as follows

$$\boldsymbol{K} = \begin{bmatrix} 0.9123 & -0.0231 & 0.1844 \\ -0.1052 & 0.8119 & -0.0567 \\ 0.0203 & -0.0192 & 0.9044 \end{bmatrix}, \quad \boldsymbol{\Omega} = \begin{bmatrix} 0.2275 & -0.0018 & 0.0083 \\ -0.0018 & 0.2471 & 0.0050 \\ 0.0083 & 0.0050 & 0.2472 \end{bmatrix}.$$

The following figures present simulation results for a DTS 50 with quantized ETC under deception attacks. Figure 11(a) shows the state trajectories $x_1(\vartheta)$, $x_2(\vartheta)$, and $x_3(\vartheta)$ under ETC with deception attacks ($\bar{\eta} = 0.3$). Starting from $x_0 = [-0.5, 2, 1]^T$, the states converge to zero by $\vartheta \approx 60$, with attack instances (30) from $y = 0$ to $y = 2$.

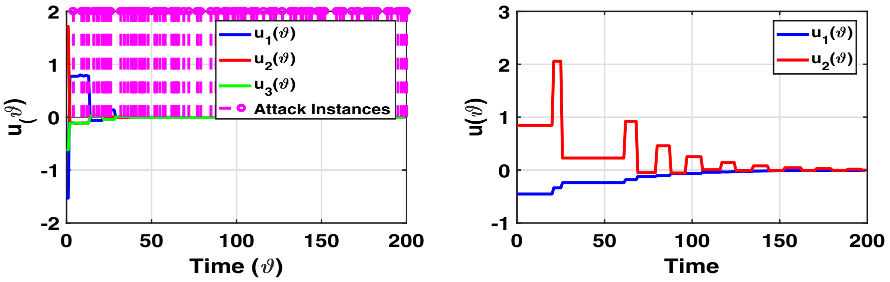

(a) With attacks (b) Without attack

Fig. 12 Control Input Responses with and without Attacks for Example 2

Fig. 13 Event-triggered release intervals for Example 2

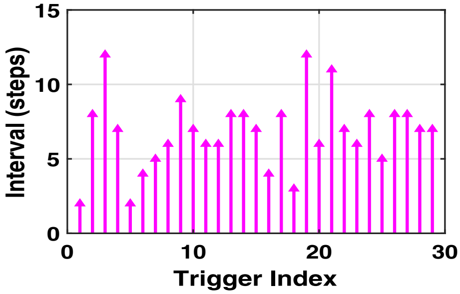

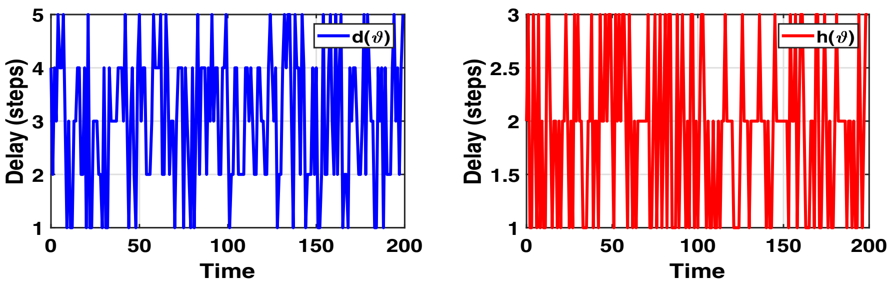

(a) variable time delay $d(\vartheta)$ (b) Network-induced delay $h(\vartheta)$

Fig. 14 Variation of Variable Time Delay $d(\vartheta)$ and Network-induced Delay $h(\vartheta)$ with Attacks for Example 2

The plot demonstrates the system's robustness to attacks. Figure 11(b) displays the state trajectories $x_1(\vartheta)$, $x_2(\vartheta)$, and $x_3(\vartheta)$ without deception attacks ($\bar{\eta} = 0$). From $x_0 = [-0.5, 2, 1]^T$, the states converge to zero by $\vartheta \approx 50$, faster than with attacks, showing nominal performance of the ETC. Figure 12(a) presents the control inputs $u_1(\vartheta)$, $u_2(\vartheta)$, and $u_3(\vartheta)$ with deception attacks ($\bar{\eta} = 0.3$). The inputs, starting from non-zero values, converge to zero as states stabilize, with 30 attack instances from $y = 0$ to $y = 2$, highlighting attack effects on control. Figure 12(b) shows the control inputs $u_1(\vartheta)$, $u_2(\vartheta)$, and $u_3(\vartheta)$ without deception attacks ($\bar{\eta} = 0$). The inputs converge to zero by $\vartheta \approx 50$, reflecting smooth control action with 30 event-triggered updates and no attack perturbations.

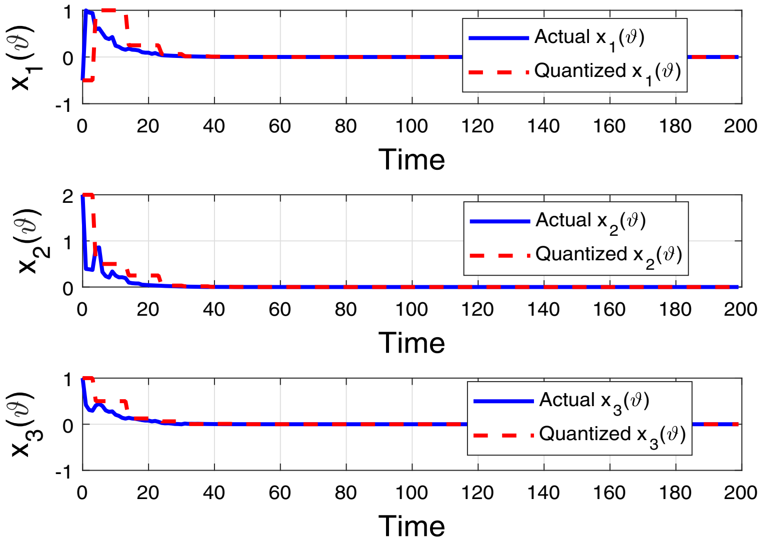

Fig. 15 Quantized vs. actual states (with attacks) for Example 2

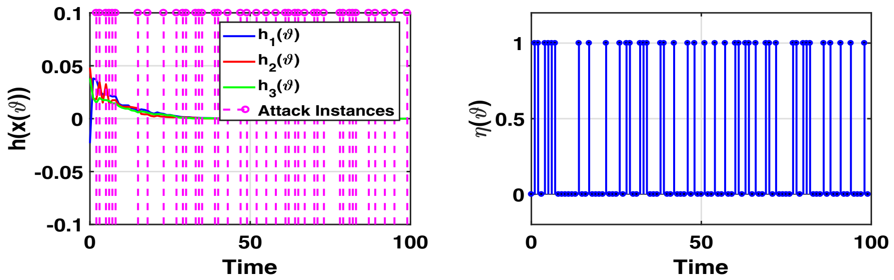

(a) $h(x(\vartheta))$ (b) $\eta(\vartheta)$

Fig. 16 Nonlinear function $h(x(\vartheta))$ and Bernoulli Distribution $\eta(\vartheta)$ (Attack Occurrences) with attacks for Example 2

Figure 13 illustrates the release intervals for the event-triggered mechanism. Figure 14(a) depicts the variable time delay $d(\vartheta)$. Plotted as a blue line, the delay varies between 1 and 5 steps randomly, illustrating its impact on system dynamics under the robust controller. Figure 14(b) shows the network-induced delay $h(\vartheta)$. Plotted as a red line, the delay varies between 1 and 3 steps randomly, reflecting network effects on state transmission in the event-triggered system. Figure 15 compares actual and quantized state trajectories $x_1(\vartheta)$, $x_2(\vartheta)$, and $x_3(\vartheta)$ with deception attacks ($\bar{\eta} = 0.3$) in three subplots. Actual states (blue, solid) and quantized states (red, dashed) converge to zero, demonstrating effective quantization despite attacks.

Figure 16(a) displays the nonlinear attack function components $h_1(\vartheta)$, $h_2(\vartheta)$, and $h_3(\vartheta)$ with deception attacks ($\bar{\eta} = 0.3$). The components converge to zero, with 30 attack instances from $y = -0.1$ to $y = 0.1$.Figure 16(b) visualizes the Bernoulli distribution $\eta(\vartheta) \in \{0, 1\}$ for deception attacks ($\bar{\eta} = 0.3$). A plot shows 30 attack

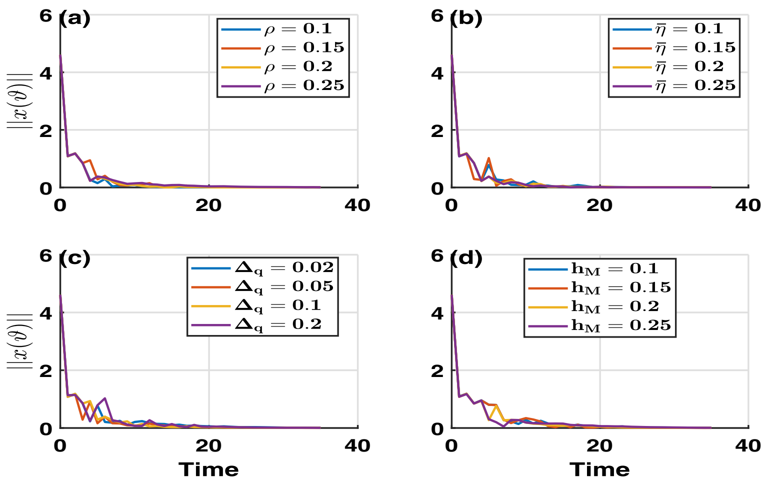

Fig. 17 "Sensitivity analysis of state norm for Example.2

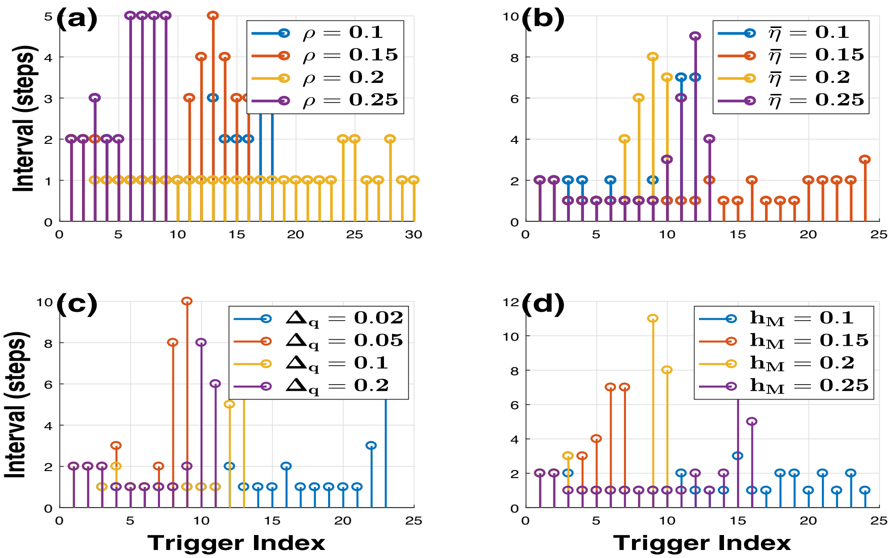

Fig. 18 Analysis of triggered interval for Example.2

occurrences, highlighting the random nature of attack events. Figure 17 shows sensitivity analysis of state norm, which depends on various values of ρ, $\bar{\eta}$, Δ_q, and h_M. Figure 18 represents sensitivity analysis of the triggered interval, which depends on different values of ρ, $\bar{\eta}$, Δ_q, and h_M.

Example 3 Consider a stirred tank reactor system [13] for analysis. Where chemical species L act to form species $O : L \to O$. Illustrated figure 19 is the system's physical configuration. Z_{Li} denotes the input concentration of the key reactant L, Z_L represents

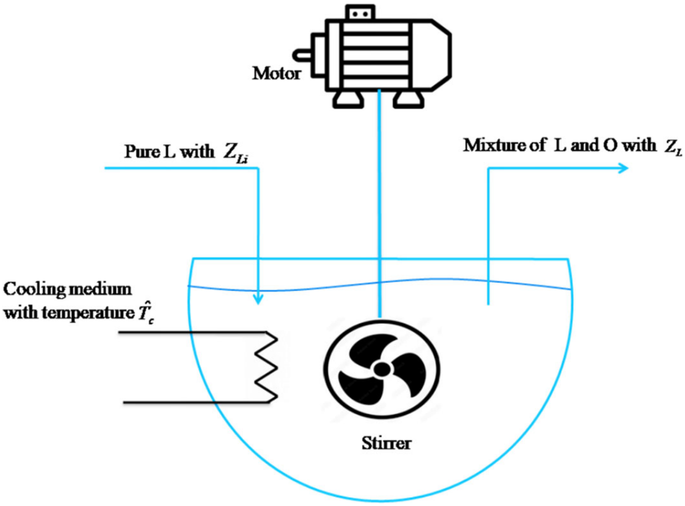

Fig. 19 A CSTR Model [13]

the output concentration of L. $\hat{T}$ is reaction temperature, $\hat{T}_c$ represents cooling medium temperature. By choosing the state and input variables as

$$\boldsymbol{x} = \begin{bmatrix} Z_L \\ \hat{T} \end{bmatrix}, u = \begin{bmatrix} \hat{T}_c \\ Z_{Li} \end{bmatrix},$$

by applying the discretized procedure with sampling period, the discretized state space model with the output signals $\boldsymbol{y}(\boldsymbol{\vartheta})$ are outlined below ($A_d = 0$).

$$\begin{cases} \boldsymbol{x}(\vartheta+1) = & \begin{bmatrix} 0.9719 & -0.0013 \\ -0.034 & 0.8628 \end{bmatrix} \boldsymbol{x}(\vartheta) + \begin{bmatrix} -0.0839 & 0.0232 \\ 0.0761 & 0.4144 \end{bmatrix} u(\vartheta) \\ & + \begin{bmatrix} -0.0839 & 0.0232 \\ 0.0761 & 0.4144 \end{bmatrix} \bar{\boldsymbol{w}}(\vartheta), \\ \boldsymbol{y}(\boldsymbol{\vartheta}) = & \begin{bmatrix} 1 & 0 \\ 0 & 0 \end{bmatrix} \boldsymbol{x}(\vartheta) + \begin{bmatrix} 0.5 \\ 0.03 \end{bmatrix} \bar{\boldsymbol{w}}(\vartheta), \end{cases} \tag{58}$$

To illustrate the performance of the proposed approach via a practical system. We assume that $h_m = 0.01$, $\bar{h} = 0.03$, $\alpha = 0.1$, $\rho = 0.12$. The ETC gains $\boldsymbol{K}$, and the triggering matrix $\boldsymbol{\Omega}$ is determined by solving the conditions described in Theorem 3 LMIs with ($A_d = 0$) assisted by the MATLAB toolbox as follows.

$$\boldsymbol{K} = \begin{bmatrix} 0.4135 & -0.0096 \\ -0.0183 & 0.0617 \end{bmatrix}, \boldsymbol{\Omega} = \begin{bmatrix} 2.9665 & 0.0872 \\ 0.0872 & 3.6937 \end{bmatrix}.$$

The following figures represent the simulation outcomes of the DTS (58) operating under quantized ETC at the presence of deception attacks. Figure 20(a) shows the state

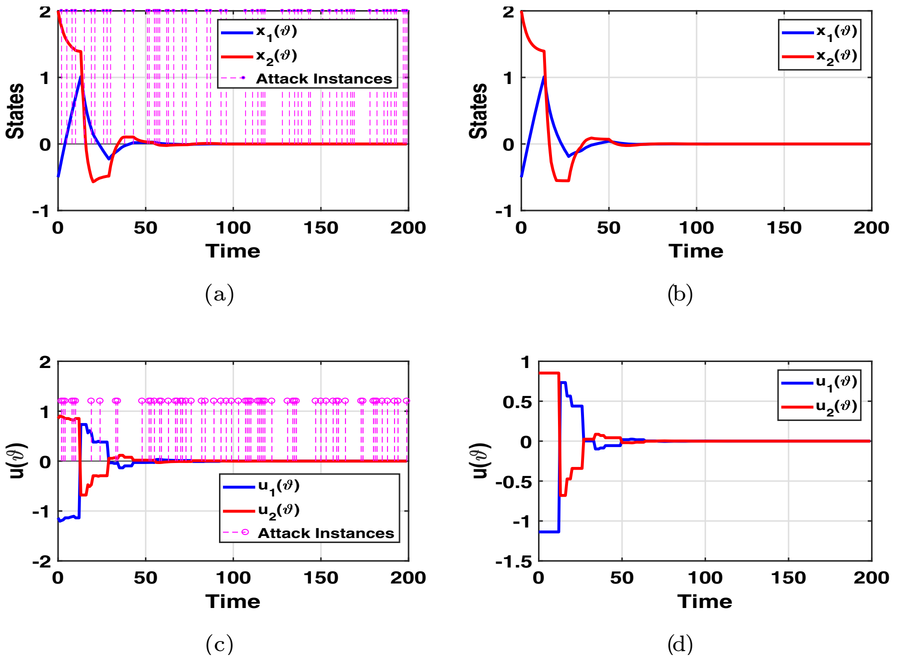

Fig. 20 Behavior of states $x_1(\vartheta)$, $x_2(\vartheta)$ and control inputs $u_1(\vartheta)$, $u_2(\vartheta)$ for Example 3

Fig. 21 The Quantized vs. actual states (with attacks) for Example 3

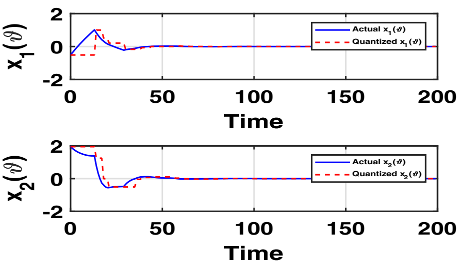

trajectories $x_1(\vartheta)$, $x_2(\vartheta)$ initial condition $[-0.5, 2]$ with deception attack $\bar{\eta} = 0.1$ converges to zero. Figure 20(b) represents the state trajectories $x_1(\vartheta)$, $x_2(\vartheta)$ starting from $[-0.5, 2]$ without deception attack converges to equilibrium point.

Figure 20(c) control inputs $u_1(\vartheta)$, $u_2(\vartheta)$ have non-zero initial values with deception attack $\bar{\eta} = 0.1$ converges to zero. Figure 20(d) addresses control inputs $u_1(\vartheta)$, $u_2(\vartheta)$ starting from non-zero values, converging to zero without deception attack. Figure 21 presents quantized and actual state trajectories. Quantized states are varied from actual state trajectories. Figure 22(a) shows the norm of the state vector, that converging to the equilibrium point. Figure 22(b) explains the norm of control input trajectories. Figure 22(c) shows ETC release intervals. Figure 22(d) represents trajectories of a non-linear function.

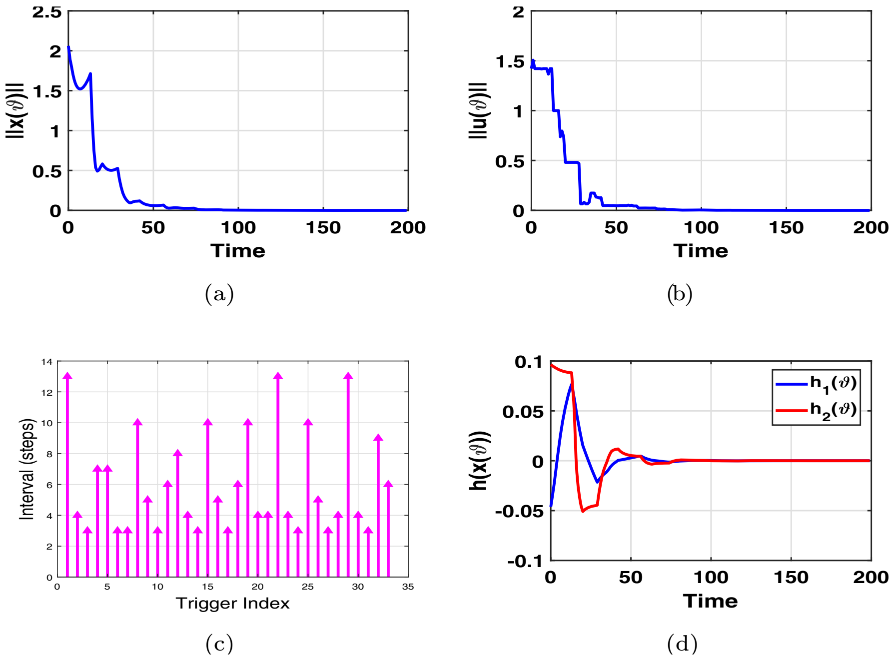

Fig. 22 (a) Norm of states; (b) Norm of control inputs; (c) Event-triggered release intervals; (d) Behavior of non-linear function of Example 3

Table 3 Triggered Rates for Example 4

ρ	0.1	0.2	0.3	0.4	0.5
Triggered rate	22 %	15.5 %	13.5 %	11.5 %	9 %

Comparison Results:

Example 4 Let us examine the DTS (50) associated with

$$\boldsymbol{A} = \begin{bmatrix} 1+0.03\Phi & 0.02\Phi \\ 0.03 & 0.2 \end{bmatrix}, \boldsymbol{A_d} = \begin{bmatrix} 0.0003 & 0.0024 \\ 0.0012 & 0.0012 \end{bmatrix}, \boldsymbol{D} = \begin{bmatrix} 0.05 & 4 \end{bmatrix},$$
$$\boldsymbol{B} = \begin{bmatrix} 0.25\Phi & 0.15\Phi \\ 0.5 & 0.4 \end{bmatrix}, \boldsymbol{F} = \begin{bmatrix} 0.15\Phi & 0.05\Phi \\ 0.05 & 0.1 \end{bmatrix}.$$

In this example, we assume that $d_l = 3, d_h = 4, \Phi = 0.05$. Based on these parameters, the LMI criteria in Theorem 3 with $\boldsymbol{E} = 0$ are evaluated, from which the related control gain matrix and triggering parameters can be derived as follows.

$$\boldsymbol{K} = \begin{bmatrix} 8.8784 & 0.3253 \\ 0.0128 & 0.3283 \end{bmatrix}, \ \boldsymbol{\Omega} = \begin{bmatrix} 1.0473 & 0.2136 \\ 0.2136 & 1.5477 \end{bmatrix}.$$

Table 4 Feasible comparison under Φ for Example.4

Φ	0.05	0.06	0.07
[16]	✓	✘	✘
Our work	✓	✓	✓

Table 5 Maximum allowable delay d_h with $d_l = 1$ for Example 4

[16]	Example 4
$d_h = 2$	$d_h = 4$

Table 6 Minimum allowable delay d_l with $d_h = 4$ for Example 4

[16]	Example 4
$d_l = 1$	$d_l = 3$

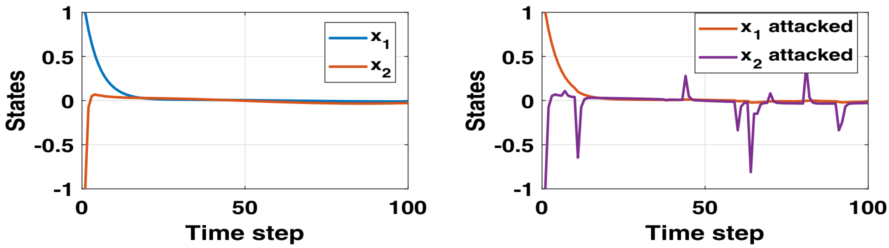

(a) without attacks

(b) with attacks

Fig. 23 State response curves without and with attacks for Example 4

Remark 4 The Table 3 represents triggering rates for different parameter ρ. The parameter increases (0.1 to 0.4), the triggering rates decrease (24.5% to 14%), indicating a reduction in communication transmissions. The Table 4 examines the feasibility of the stability conditions for different values of the parameter Φ (0.05, 0.06, and 0.07). The proposed LMI conditions remain feasible for $\Phi = 0.05, 0.06, 0.07$, demonstrating robustness. The Table 5 provides that with $d_l = 1$, the proposed method allows a larger maximum delay $d_h = 4$ compared to 2 in reference [16], indicating reduced conservatism. The Table 6 presents that with $d_h = 4$, the minimum allowable delay bound is improved compared to [16], further Figs. 23, 24, and 25 represents the state trajectories, control input responses, and the event-triggered release intervals for Example 4.

5 conclusion

In this paper, we have proposed a general class of approaches to tackle the problem of preserving passivity against disturbance under quantized event-triggered communication in delayed discrete-time systems subject to deception attacks. To lower the communication rate and the burden of the network, an event-triggered policy and a logarithmic quantizer were applied. Quantization and event-triggering/cyber attacks

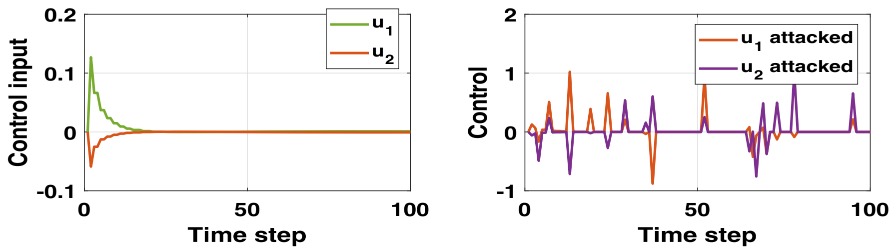

(a) without attack

(b) with attacks

Fig. 24 Control input responses without and with attacks for Example 4

Fig. 25 Event-triggered release intervals for Example 4

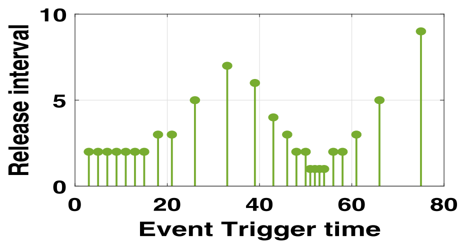

were taken into account at the same time, both considered in an atomic control framework. Through constructing a proper LKF, sufficient conditions in terms of LMIs were derived to guarantee the asymptotic stability and passivity of the system. An ETC law was also developed by remote centralized control for stable operation with the aid of event-triggering in the presence of communication constraints. The effectiveness of the proposed method is demonstrated by four numerical examples, which illustrate that the system stability as well as the passivity can be preserved successfully with much reduced communication. These results demonstrate the application feasibility and enhanced performance of the proposed control scheme. The limitation of the proposed method is Lemma 1 and Lemma 2, which increases the computational complexity. Nevertheless, Lemma 1 and Lemma 2 are introduced in certain cases to obtain more admissible solutions and enlarge the feasible solution region. The controller feedback matrices are calculated from the feasible solutions of the corresponding LMIs whenever the proposed conditions are feasible. It is worth noting that the results of this paper are compared with the existing ones in the literature. The proposed method can also be applied to more challenging problems, such as filtering and observer design, as well as systems with external disturbances including dissipativity, passivity, and H_∞ performance. Additionally, the possible extension of the presented work to switched systems, discrete time Markovian jumps neural network, and synchronization for a discrete time power system.

Author Contributions All authors contributed equally and significantly to the writing of this article and typed, read, and approved the final manuscript.

Funding Not applicable

Data Availability No datasets were generated or analyzed during the current study.

Declarations

Conflicts of Interest The authors declare no Conflict of interest.

References

1. M. Aoki, *Optimization of Stochastic Systems: Topics in Discrete-time Systems*. Elsevier (2016)
2. N. Cho, H.-S. Shin, A passivity-based method for accelerated convex optimisation. In: 2024 IEEE 63rd Conference on Decision and Control (CDC), pp. 5503–5508. IEEE (2024)
3. H. Fatoorehchi, S. Djilali, Stability analysis of linear time-invariant dynamic systems using the matrix sign function and the adomian decomposition method. Int. J. Dyn. Control **11**(2), 593–604 (2023)
4. H. Fatoorehchi, P.L. Fosbøl, On the maximum horizontal distance of a matrix's eigenvalues from the imaginary axis: a new criterion for control system stability. J. Franklin Inst. **363**(1), 108258 (2025)
5. H. Gao, T. Chen, New results on stability of discrete-time systems with time-varying state delay. IEEE Trans. Autom. Control **52**(2), 328–334 (2007)
6. X. Ge, Q.-L. Han, L. Ding, Y.-L. Wang, X.-M. Zhang, Dynamic event-triggered distributed coordination control and its applications: a survey of trends and techniques. IEEE Trans. Syst. Man Cybern. Syst. **50**(9), 3112–3125 (2020)
7. Y. He, M. Wu, G.-P. Liu, J.-H. She, Output feedback stabilization for a discrete-time system with a time-varying delay. IEEE Trans. Autom. Control **53**(10), 2372–2377 (2008)
8. A. Keymasi-Khalaji, M. Haghjoo, Passivity-based stabilizing controller for an underwater robot. Ocean Eng. **302**, 117656 (2024)
9. D. Larby, F. Forni, Optimal virtual model control for robotics: Design and tuning of passivity-based controllers. Preprint at arXiv:2411.06627 (2024)
10. F. Li, Z. Ding, N. He, Parameter learning for wiener systems with time-delay state-space model. Asian J. Control **27**(1), 179–190 (2025)
11. F. Li, J. Han, N. He, Q. Cao, L. Xu, Parameter identification for the hammerstein-wiener nonlinear time delay systems with process noises. Circuits Systems Signal Process. **44**(3), 1726–1752 (2025)
12. F. Li, Y. Zhu, S. Zhou, Q. Cao, Parameters estimation of hammerstein-wiener time-delay nonlinear model. Trans. Inst. Meas. Control. 01423312251361674 (2025)
13. H. Liu, X.-J. Li, C. Deng, C.K. Ahn, Fault estimation and control for unknown discrete-time systems based on data-driven parameterization approach. IEEE Trans. Cybern. **53**(3), 1629–1640 (2021)
14. Y. Liu, Z. Fang, J.H. Park, F. Fang, Quantized event-triggered synchronization of discrete-time chaotic neural networks with stochastic deception attack. IEEE Trans. Syst. Man Cybern. Syst. **53**(7), 4511–4521 (2023)
15. H. Ma, H. Li, R. Lu, T. Huang, Adaptive event-triggered control for a class of nonlinear systems with periodic disturbances. Science China Inf. Sci. **63**(5), 150212 (2020)
16. L. Ma, Z. Wang, C. Cai, F.E. Alsaadi, A dynamic event triggered approach to H_∞ control for discrete-time singularly perturbed systems with time-delays and sensor saturations. IEEE Trans. Syst. Man Cybern. Syst. **51**(11), 6614–6625 (2020)
17. M.S. Mahmoud, A. Ismail, Resilient control of non-linear discrete time state-delay systems. Appl. Math. Comput. **206**(2), 561–569 (2008)
18. J. Miao, *Economic Dynamics in Discrete Time*. MIT press (2020)
19. R. Ortega, J.G. Romero, P. Borja, A. Donaire, PID passivity-based control of nonlinear systems with applications. John Wiley & Sons (2021)
20. S. Pandey, S. Tadepalli, S. Bhusnur, R. Nigam, Improved stability and passivity results for discrete time-delayed systems with saturation nonlinearities and external disturbances. Circuits Systems Signal Process. **43**(1), 103–123 (2024)
21. S.-B. Qiu, X.-G. Liu, F.-X. Wang, Q. Chen, Stability and passivity analysis of discrete-time linear systems with time-varying delay. Syst. Control Lett. **134**, 104543 (2019)
22. R. Sakthivel, S. Santra, B. Kaviarasan, Resilient sampled data control design for singular networked systems with random missing data. J. Franklin Inst. **355**(3), 1040–1072 (2018)
23. M. Susca, V. Mihaly, Z. Lendek, I.-C. Morarescu, A passivity analysis tool for linear clustered multi-agent systems. IEEE Control Syst. Lett. **9**, 739–744 (2025)

24. H.M. Sweatland, A. Isaly, E.J. Griffis, W.E. Dixon, Optimization-based controllers for passivity and safety constraints. IEEE Trans. Autom. Control **70**(5), 3339–3345 (2024)
25. R. Vadivel, M.S. Ali, Y.H. Joo, Event-triggered H_∞ synchronization for switched discrete time delayed recurrent neural networks with actuator constraints and nonlinear perturbations. J. Franklin Inst. **357**(7), 4079–4108 (2020)
26. R. Vadivel, P. Hammachukiattikul, N. Gunasekaran, R. Saravanakumar, H. Dutta, Strict dissipativity synchronization for delayed static neural networks: an event-triggered scheme. Chaos, Solitons & Fractals **150**, 111212 (2021)
27. R. Vadivel, P. Hammachukiattikul, Q. Zhu, N. Gunasekaran, Event-triggered synchronization for stochastic delayed neural networks: passivity and passification case. Asian J. Control **25**(4), 2681–2698 (2023)
28. R. Vadivel, S. Sabarathinam, G. Zhai, N. Gunasekaran, Event-triggered reachable set estimation for synchronization of markovian jump complex-valued delayed neural networks under cyber-attacks. Eur. Phys. J. Special Topics, 1–21 (2024)
29. R. Vadivel, M.S. Ali, Y.H. Joo, Robust H_∞ performance for discrete time T-S fuzzy switched memristive stochastic neural networks with mixed time varying delays. J. Exp. Theor. Artif. Intell. **33**(1), 79–107 (2021)
30. X. Xiao, J.H. Park, L. Zhou, G. Lu, Event-triggered control of discrete-time switched linear systems with network transmission delays. Automatica **111**, 108585 (2020)
31. X. Yang, J. Zhang, E. Fridman, Periodic averaging of discrete time systems: a time-delay approach. IEEE Trans. Autom. Control **68**(7), 4482–4489 (2022)
32. J. Zhang, Y. Xia, Z. Sun, D. Chen, *Networked and Event-triggered Control Approaches in Cyber-physical Systems*. CRC Press (2022)
33. K. Zhang, L. Zhang, L. Xie, *Discrete-time and Discrete-space Dynamical Systems*. Springer (2020)
34. D. Zhao, Z. Wang, D.W. Ho, G. Wei, Observer-based PID security control for discrete time-delay systems under cyber-attacks. IEEE Trans. Syst. Man Cybern. Syst. **51**(6), 3926–3938 (2019)